J. Fluid Mech. (1984), *vol.* 144, *pp.* 47–77
Printed in Great Britain

Three-dimensional viscous flows with large secondary velocity

By W. R. BRILEY AND H. McDONALD
Scientific Research Associates, Inc., Glastonbury, CT 06033, U.S.A.

(Received 8 August 1983 and in revised form 20 February 1984)

A new system of approximating equations is derived for three-dimensional steady viscous compressible flows in which a primary flow direction is present, but in which both transverse velocity components can be large. If the transverse velocity vector which corrects a given potential flow is first decomposed into 'potential' and 'rotational' *vector* components, then a re-examination of three-dimensional boundary-layer theory shows that both components (v_ϕ, w_ϕ) of the potential-velocity vector may be assumed small, whereas both components (v_ψ, w_ψ) of the rotational-velocity vector and hence of the composite secondary flow (v, w) can remain of order unity. An assumption of small scalar potential then leads to a system of governing equations whose characteristic polynomial has a non-elliptic form for arbitrary Mach number, without introducing any direct approximation of either streamwise or transverse pressure gradient terms. These non-elliptic equations can be solved very economically as a well-posed initial/boundary-value problem. Computed results for laminar subsonic flow in a curved square duct confirm the small scalar-potential approximation for both large ($R/d = 100$) and small ($R/d = 2$) radius of curvature. Other computations for $R/d = 2.3$ are in good agreement with the measurements of Taylor, Whitelaw & Yianneskis (1980).

1. Introduction

A predominant direction of flow can be identified in many high-Reynolds-number flow problems. This primary flow direction may derive from the direction of flight in external aerodynamics or from the ducted nature of many internal flows. Many of these flows are inherently three-dimensional because of geometry and/or other factors. When viscous effects or other sources of vorticity are present, three-dimensional flows differ fundamentally from their two-dimensional counterparts in that large secondary flows are easily generated by a deflection of the primary flow and/or by other mechanisms. Secondary-flow theory (reviewed by Horlock & Lakshminarayana 1973; Lakshminarayana & Horlock 1973) affords considerable insight into the generation of secondary flow and establishes that streamwise vorticity on the order of 50% of the transverse vorticity (shear) can be generated by a lateral flow deflection of only 15°. The large secondary flows thus generated often exert an appreciable influence on the primary flow, and thus aerodynamic performance, viscous flow losses and heat transfer can be affected significantly.

The general complexity of three-dimensional viscous flows has led to a heavy emphasis on analytical methods which eventually lead to the numerical solution of governing partial differential equations. In the present paper, a new system of approximating equations is derived for steady three-dimensional viscous compressible flows in which a primary-flow direction with no significant flow reversal is present.

but in which either or both transverse velocity components can be of order unity. The solution of these equations can be accomplished by economical forward-marching numerical algorithms, and without the need for global iteration procedures.

1.1. *Related computational approaches*

The present discussion will focus on physical approximations and their general effect on computational labour, but will not address numerical approximations or the error and labour of specific algorithms. Although solution of the Navier–Stokes equations is feasible and has been demonstrated in three dimensions (e.g. Williams 1969; Briley & McDonald 1977; Humphrey, Taylor & Whitelaw 1977; Hah 1983), the labour of solution using presently available algorithms is considerable for high-Reynolds-number flows with multiple length-scales requiring locally refined three-dimensional meshes. For this reason there is an extensive literature which addresses simplification of the steady Navier–Stokes equations for the purpose of numerical solution, often for application to high-Reynolds-number flows without streamwise flow reversal. A portion of this literature is reviewed by Davis & Rubin (1980); other discussion can be found in references given here. All of the approaches considered here neglect streamwise diffusion in some manner.

The goal of these approaches has been to achieve a level of approximation that would yield accurate flow predictions, while reducing the labour of solution below that of the Navier–Stokes equations. The computational labour is greatly influenced by the type of governing equations solved, and here it is important to note that terminology such as 'parabolic' and 'elliptic' has been interpreted differently by different authors. The variations in terminology seem to derive from a scalar viewpoint which associates each momentum equation with a given velocity component, instead of considering the system of equations as a whole. For the purposes of the present paper, the term 'elliptic' is applied to *systems* of equations whose characteristic polynomial has one or more imaginary roots, and systems for which no imaginary roots occur are referred to as 'non-elliptic'. This is discussed further in §3 and in Appendix A. Computationally, the distinction is very important, since elliptic systems are generally ill-posed for solution as an initial/boundary-value problem, whereas non-elliptic systems are solvable by much more economical forward-marching algorithms. Clearly, there is ample motivation to seek approximations of reasonable accuracy which offer the computational economy associated with non-elliptic approximating equations.

An assumption that one or both transverse velocity components is small (in some coordinate system) has often led to non-elliptic approximating equations. The two-dimensional boundary layer is a well-known example, where the usual order-of-magnitude estimates justify neglecting all convective and viscous terms in the normal (y) momentum equation. If coordinate curvature terms are absent or neglected, then this equation reduces to $\partial p/\partial y = 0$, which can be integrated to obtain $p = p(x)$ and introduced as a pressure approximation in the x-momentum equation. If significant curvature terms are present, as in the slender- (but curved-) channel approximations of Blottner (1977) and Anderson (1980), then the y-momentum equation can no longer be integrated to approximate the streamwise pressure-gradient term, and must be solved treating pressure as a dependent variable. Either approximation produces non-elliptic equations, however, since coordinate curvature terms do not affect the analysis of characteristics. The same is true for three-dimensional boundary layers, and non-elliptic equations are obtained when convective and

viscous terms are neglected in the y-momentum equation, whether or not the streamwise pressure-gradient term is approximated using $p = p(x, z)$.

If both transverse velocity components are small in a three-dimensional flow, and if curvature terms are negligible, then the transverse momentum equations reduce to $\partial p/\partial y = 0$ and $\partial p/\partial z = 0$, and this justifies an approximation $p = p(x)$ in the x-momentum equation which produces non-elliptic equations. The analysis of Rubin, Khosla & Saari (1977) for entry flow in straight ducts contains an example of this type. Other approaches that assume that both transverse velocity components are small are discussed by Baker & Orzechowski (1983) and Anderson & Hankins (1981).

In the flows addressed here, both transverse velocity components may be large, significant curvature terms may be present, and the geometry may contain streamwise corners in which the surface normal changes direction. Conventional boundary layer arguments based on a small normal velocity component are clearly not applicable in these circumstances. For this type of flow, many authors have instead used an approximation based on a multiple definition of pressure, in which the streamwise pressure gradient has a known form, but is completely independent of the transverse pressure-gradient terms. Although not based on order-of-magnitude estimates, this approximation has been found to produce non-elliptic equations and has been used, for example, by Patankar & Spalding (1972), Carreto, Curr & Spalding (1973), Briley (1974), Ghia & Sokhey (1977), Kreskovsky, Briley & McDonald (1981) and Levy, Briley & McDonald (1983). In the authors' experience, this particular approximation can provide reasonable accuracy for many problems if the streamwise pressure gradient is represented by a potential-flow pressure with a mean-pressure correction, and with no approximation introduced for transverse pressure gradients. Nevertheless, the multiple definition of pressure does not allow the streamwise momentum balance to be influenced by experimentally observed distortions of the static pressure field, which are induced by large secondary flows.

One approach which avoids approximations in pressure-gradient terms neglects *only* streamwise diffusion terms in the Navier–Stokes equations. This approximation is not very restrictive and only requires a coordinate system aligned with shear layers; these equations are also suitable for problems with reversed flow. The diverse approaches of Pratap & Spalding (1976), Moore & Moore (1979), Pulliam & Steger (1980) and Rubin & Reddy (1983) are all based on these approximating equations, which are often termed the parabolized or thin-layer Navier–Stokes equations. Although the neglect of streamwise diffusion is often described as a parabolizing approximation, it is generally agreed that in subsonic-flow regions these governing equations are in some sense 'elliptic' unless further approximation is introduced, usually in the streamwise pressure gradient. This is discussed, for example, by Davis & Rubin (1980), and the case of mixed supersonic/subsonic flow has been studied by Vigneron, Rakich & Tannehill (1978) and Schiff & Steger (1980) among others. If forward-marching algorithms are used when only streamwise diffusion is to be neglected, then these algorithms are normally used within a context of global iteration analogous to that employed in time-like or other global iteration algorithms for the Navier–Stokes equations. A classification based on relevant viscous and inviscid characteristic equations is given in Appendix A for most of the approximating equations considered here, in their incompressible form.

In the present paper the boundary-layer order-of-magnitude estimates are re-examined in terms of a transverse velocity which has been decomposed into potential (v_ϕ, w_ϕ) and rotational (v_ψ, w_ψ) components which are themselves vectors, instead of

the usual representation in terms of the velocity components v and w. It is found that the potential-velocity vector must be small when either transverse coordinate can be the surface normal of a boundary layer, whereas the rotational-velocity vector can be of order unity and parallels the growth in streamwise vorticity. The potential- and rotational-velocity vectors thus have the same role in deriving approximations for a viscous secondary flow as the 'normal' and 'crossflow' velocity components in a three-dimensional boundary layer. An assumption of small scalar potential then leads to viscous approximations neglecting streamwise diffusion, and inviscid approximations affecting convective terms in the transverse momentum equations and stagnation enthalpy. On examination of the characteristic polynomial, it is found that the viscous approximation *alone* is sufficient to produce a parabolic system of equations. However, the presence of essentially inviscid-flow regions at high Reynolds number suggests that the approximations used should also reduce the Euler equations to a non-elliptic form. The present inviscid approximations reduce the compressible Euler equations to a non-elliptic form for arbitrary Mach number. The resulting non-elliptic approximating equations can then be solved as an initial/boundary-value problem, with a consequent saving in computer resources. Although the approximations introduced here appear to have a wider range of applicability which includes both internal- and external-flow problems, the present investigation is restricted to laminar subsonic flow in a square duct having appreciable streamwise curvature.

2. Derivation of the small-scalar-potential approximation

2.1. *Compressible Navier–Stokes equations*

In the present notation all variables are non-dimensional, having been normalized by reference quantities denoted by a subscript r, and all vectors are identified by boldface type. The continuity equation is given by

$$\nabla\cdot\rho\boldsymbol{U} = 0 \tag{2.1}$$

where ρ is density and $\boldsymbol{U}$ is velocity. The momentum equation is expressed in vector form as $\rho\boldsymbol{M} = 0$, where

$$\boldsymbol{M} \equiv (\boldsymbol{U}\cdot\nabla)\boldsymbol{U} + \rho^{-1}\nabla p - Re^{-1}\boldsymbol{F} = 0. \tag{2.2}$$

Here p denotes pressure, and $\boldsymbol{F}$ denotes force due to viscous stress. The reference pressure p_r has been taken as $\rho_r U_r^2$, and the Reynolds number Re is defined by $Re = \rho_r U_r L_r/\mu_r$, where L denotes length and μ denotes molecular viscosity. The equation of state for a perfect gas may be written as

$$p = \rho T/\gamma M_r^2, \tag{2.3}$$

and the total enthalpy E is defined by

$$E = T + \tfrac{1}{2}(\gamma-1)\,M_r^2 q^2 \tag{2.4}$$

where $q^2 \equiv \boldsymbol{U}\cdot\boldsymbol{U}$. Here T denotes temperature, and the reference enthalpy E_r has been taken as $C_p T_r$, where C_p is specific heat at constant pressure. The reference Mach number M_r is defined by $M_r = U_r/c_r$, where c_r is the reference speed of sound defined by $c^2 = \gamma R T_r$, and where γ is the specific-heat ratio and R is the gas constant. The energy equation can be expressed in terms of total enthalpy as

$$\rho\boldsymbol{U}\cdot\nabla E = (Re\,Pr)^{-1}\nabla\cdot k\nabla E + (\gamma-1)\,M_r^2\,Re^{-1}\,[\mu\Phi + \rho\boldsymbol{U}\cdot\boldsymbol{F} - Pr^{-1}\nabla\cdot k\nabla\tfrac{1}{2}q^2], \tag{2.5}$$

where Φ is the dissipation function, k is thermal conductivity, and the Prandtl number Pr is defined by $Pr = C_p \mu_r / k_r$. Note that temperature T does not appear in the energy equation (2.5). The temperature can also be eliminated from the state equation by combining (2.3) and (2.4), giving

$$p = \frac{\rho E}{\gamma M_r^2} - \frac{(\gamma - 1)\rho q^2}{2\gamma}. \tag{2.6}$$

There are two advantages to the formulation given here. First, if μ and k are zero, then the energy equation (2.5) states that the total enthalpy E is constant along streamlines. In many compressible flows with negligible heat transfer and with $Pr \approx 1$, E can be assumed to be a known constant E_0. The energy equation can then be omitted from consideration, since (2.6) is sufficient to relate density to pressure and velocity, and thus close the system of equations. If the total enthalpy is not constant, then the energy equation is solved. The second advantage is that this formulation is well behaved at low Mach number. This was shown by Briley, McDonald & Shamroth (1983), by noting that if a pressure coefficient $\frac{1}{2}C_p \equiv p - 1/\gamma M_r^2$ is introduced, then for constant total enthalpy this compressible formulation reduces to the incompressible ($\rho = 1$) equations in the limit $M_r \to 0$.

In the development that follows, the coordinates x, y, z, velocity components u, v, w, and the unit vectors $\boldsymbol{i}_1$, $\boldsymbol{i}_2$, $\boldsymbol{i}_3$ in the x-, y- and z-directions respectively, refer to a general orthogonal coordinate system. The metric coefficients are denoted h_1, h_2 and h_3.

2.2. *Physical background*

The viscous developing flow in a rectangular duct whose centreline has appreciable curvature is representative of the primary/large-secondary flow structure of interest here, and provides an orientation and physical basis for the present flow approximations. The corresponding (incompressible) entry flow in a straight square duct has been considered in some detail by Rubin *et al.* (1977). Excluding a small region of axial extent Re^{-1} near the leading edge, the flow structure in the straight duct consists of boundary layers, corner-layer regions, and a potential-core region with displacement interaction (blockage) effects. Further downstream, the flow structure evolves into a fully viscous region where the boundary-layer, corner-layer and potential-core regions merge and become less distinct. Eventually, the flow becomes fully developed and independent of axial distance.

If the duct centreline is given an appreciable curvature in the region where thin boundary and corner layers are present, a different flow structure evolves. The potential flow for this curved geometry has radial pressure gradients beginning about one to two hydraulic diameters upstream of the bend, and three-dimensional boundary layers thus form on the endwalls, with large radial crossflow toward the inside corners of the bend. A schematic of the cross flow behaviour near the change in curvature is shown in figure 1, as deduced from flow-visualization experiments and other sources. Since the flow is confined, the crossflow is deflected in the corner and returns to the centre region of the duct. A corner-vortex structure may be formed, depending on the flow parameters present. As indicated in figure 1, the outer portion of the boundary-layer and corner-flow regions away from the walls behaves as a rotational inviscid flow region in which secondary flow is generated (in the terminology of secondary-flow theory) by turning of the transverse vorticity (shear). Viscous effects are limited to the region very near the wall. This initial behaviour of the endwall boundary layer near the change in duct curvature is consistent with empirical observations of boundary-layer velocity profiles having triangular polar diagrams

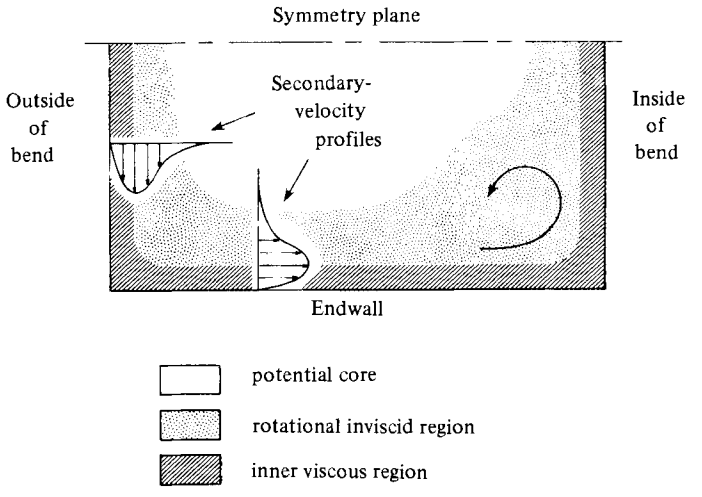

FIGURE 1. Schematic of a secondary-flow structure near start of bend.

(e.g. Johnston 1960). The rotational inviscid behaviour is also reminiscent of the middle rotational inviscid layer of triple-deck theory for a two-dimensional boundary layer subjected to a streamwise disturbance, although the latter case does not involve streamwise vorticity. As the flow proceeds downstream, the secondary flow convects the streamwise vorticity and distorts the primary flow in what amounts to a strong interaction in transverse directions between viscous and inviscid (rotational or potential) flow regions. Significant regions of rotational but essentially inviscid flow occur as a result of this process, and the potential-core region will eventually disappear. If the duct curvature is constant, an incompressible flow can eventually reach a state of fully developed curved flow.

Finally, it has been known for some time that measured static pressure distributions tend to depart significantly from the potential-flow pressure when large secondary flows are present. This is clear, for example, from the measurements of Stanitz, Osborn & Mizisin (1953) in a strongly curved duct, where the measured static pressure is three-dimensional near the inside corners of the duct, even though the potential flow for this particular geometry is two-dimensional. This behaviour is in contrast with a two-dimensional flow with small transverse velocity, where the modification of the potential-flow pressure due to viscous interaction is often slight unless separation is present.

The present analysis introduces approximations which are consistent with an evolving flow structure of the type just described. Because of the strong interrelation of the potential-core region, rotational inviscid region and viscous region near walls, a single set of approximate equations will be derived for simultaneous application to all of these flow regions at each transverse plane.

2.3. *Secondary-velocity decomposition*

The x-coordinate is chosen here to identify the primary-flow direction, and the secondary flow occurs in the transverse (normal) (y, z)-coordinate surfaces. The secondary (transverse) velocity components are first formulated as a correction to a known potential flow solution for the geometry of interest. These correction velocities, which arise from viscous effects and secondary flows, are not assumed to be small; instead, approximations based on a small scalar-potential contribution to

these correction velocities will be derived. The velocity components and pressure from this potential flow are known quantities denoted U, V, W, and P. The transverse velocity components V and W from the potential flow incorporate downstream information from the geometry and boundary conditions, and this together with the choice of coordinates is the only means by which downstream conditions are represented in the analysis. Transverse velocity corrections δv, δw are introduced as follows:

$$v = V + \delta v, \quad w = W + \delta w, \tag{2.7}$$

and the velocity vector $\boldsymbol{U}$ is then written as

$$\boldsymbol{U} = \boldsymbol{i}_1 u + \boldsymbol{U}_s + \delta \boldsymbol{U}_s \tag{2.8}$$

where u is the primary (streamwise) velocity component, and $\boldsymbol{U}_s$ and $\delta \boldsymbol{U}_s$ are transverse velocity vectors defined by

$$\boldsymbol{U}_s = \boldsymbol{i}_2 V + \boldsymbol{i}_3 W, \tag{2.9}$$

$$\delta \boldsymbol{U}_s = \boldsymbol{i}_2 \delta v + \boldsymbol{i}_3 \delta w. \tag{2.10}$$

Approximate equations governing u, δv, δw and p (and for compressible flow ρ and E) will be derived subsequently. The purpose of (2.7) is to define the approximations relative to V and W from the potential flow, independent of the streamwise coordinate direction. If the x-coordinate is aligned with the potential flow streamlines, then V and W are identically zero, and (2.7) is a simple redefinition.

In deriving the present approximating equations, care will be taken to ensure that the final equations have the property that for zero viscosity and inviscid boundary conditions, the analysis can recover the potential flow solution by a forward-marching calculation (i.e. $u, v, w, p \rightarrow U, V, W, P$). This occurs because the approximations are exact when δv, δw are zero, giving $v, w \rightarrow V, W$, and for incompressible flow u and p are then determined without approximation by the continuity and x-momentum equations. This property is retained if the potential flow is compressible, since the analysis then yields constant total enthalpy (for adiabatic flow), with density determined algebraically by the equation of state. Likewise, if an Euler solution is available, it can be used in place of the potential flow, although a potential flow is much more economical to compute.

The secondary velocity correction $\delta \boldsymbol{U}_s$ is now replaced by the following vector-field decomposition:

$$\delta \boldsymbol{U}_s = \boldsymbol{\nabla}_s \phi + \rho^{-1} \boldsymbol{\nabla} \times \boldsymbol{i}_1 \psi \tag{2.11}$$

where $\boldsymbol{\nabla}_s$ is the (transverse) surface gradient operator, which is given for orthogonal coordinates by

$$\boldsymbol{\nabla}_s = \boldsymbol{i}_2 \frac{1}{h_2} \frac{\partial}{\partial y} + \boldsymbol{i}_3 \frac{1}{h_3} \frac{\partial}{\partial z}. \tag{2.12}$$

The decomposition (2.11) defines the two components of an arbitrary vector $\delta \boldsymbol{U}_s$ in the (y, z)-surface, and is thus equivalent to a change in dependent variables from $\delta v, \delta w$ to ϕ, ψ. The analysis and notation are simplified if (2.11) is rewritten as

$$\delta \boldsymbol{U}_s = \boldsymbol{U}_\phi + \boldsymbol{U}_\psi \tag{2.13}$$

where $\boldsymbol{U}_\phi$ and $\boldsymbol{U}_\psi$ are the ϕ- and ψ-components respectively of $\delta \boldsymbol{U}_s$. The (composite) transverse velocity components in (2.7) can now be expressed as

$$v = V + v_\phi + v_\psi, \quad w = W + w_\phi + w_\psi, \tag{2.14}$$

where v_ϕ, w_ϕ and v_ψ, w_ψ are the components of $\boldsymbol{U}_\phi$ and $\boldsymbol{U}_\psi$ respectively. The vectors $\boldsymbol{U}_\phi$ and $\boldsymbol{U}_\psi$ satisfy the following identities of the decomposition:

$$\boldsymbol{i}_1 \cdot \nabla \times \boldsymbol{U}_\phi \equiv 0, \tag{2.15}$$

$$\nabla \cdot \rho \boldsymbol{U}_\psi \equiv 0. \tag{2.16}$$

The form of (2.15) and (2.16) suggests a physical interpretation for the ϕ- and ψ-components of the secondary velocity. From (2.15), $\boldsymbol{U}_\phi$ does not contribute to the streamwise component of vorticity, whereas (2.16) shows that the continuity equation is satisfied for arbitrary $\boldsymbol{U}_\psi$. Thus $\boldsymbol{U}_\psi$ is the secondary velocity induced by streamwise vorticity, whereas $\boldsymbol{U}_\phi$ is generated through continuity by the streamwise gradient $\partial \rho u / \partial x$.

In Cartesian coordinates and with $\rho = 1$, the correction velocities take the simple form

$$v_\phi = \frac{\partial \phi}{\partial y}, \quad w_\phi = \frac{\partial \phi}{\partial z}, \quad v_\psi = \frac{\partial \psi}{\partial z}, \quad w_\psi = -\frac{\partial \psi}{\partial y} \tag{2.17a–d}$$

in which ϕ and ψ have the same definitions as the conventional velocity potential (ϕ) and stream function (ψ) for two-dimensional flow in the (y, z)-plane. Rubin *et al.* (1977) employed the change of variables (2.17*a–d*) in their study of incompressible entry flow in straight ducts, because of advantages that arise in devising numerical algorithms (also exploited here). The velocity decomposition (2.11) extends this change in variables to general orthogonal coordinates and nonconstant density, by interpreting ϕ as a scalar 'surface' potential, and $\boldsymbol{i}_1 \psi$ as a vector 'surface' potential. This velocity decomposition will later provide a means for introducing new flow approximations which lead to a non-elliptic system of equations. Finally, for two-dimensional flow in the (x, y)-plane, the only non-zero component in (2.17*a–d*) is v_ϕ. Although the use of (2.17*a*) in two dimensions is not necessary in the present context, in the composite-velocity formulation of Khosla & Rubin (1983) this expression is supplemented by $u = (1 + \partial \phi / \partial x)\, U(x, y)$ and is used to devise a numerical algorithm for the Navier–Stokes equations.

2.4. *Order of magnitude estimates*

To guide the present flow approximations, it is instructive to re-examine the order-of-magnitude estimates from conventional three-dimensional boundary-layer theory, as they apply to the decomposed secondary velocity in (2.11). For simplicity (but ultimately without loss of generality), it is sufficient to consider a streamwise coordinate aligned with the potential flow, such that $V = W = 0$. In this case, the decomposed transverse velocity components are given by

$$v = v_\phi + v_\psi = \frac{1}{h_2}\frac{\partial \phi}{\partial y} + \frac{1}{h_1 h_3 \rho}\frac{\partial h_1 \psi}{\partial z}, \tag{2.18}$$

$$w = w_\phi + w_\psi = \frac{1}{h_3}\frac{\partial \phi}{\partial z} - \frac{1}{h_1 h_2 \rho}\frac{\partial h_1 \psi}{\partial y}. \tag{2.19}$$

Taking δ as the shear layer thickness and assuming that h_1, h_2, h_3 are $O(1)$ quantities, the following order-of-magnitude estimates are made in three-dimensional boundary layer theory.

If y is taken as the coordinate normal to the wall then

$$\rho, u, w, \frac{\partial}{\partial x}, \frac{\partial}{\partial z} = O(1), \quad v = O(\delta), \quad \frac{\partial}{\partial y} = O(\delta^{-1}). \tag{2.20}$$

If z is taken as the normal coordinate then

$$\rho, u, v, \frac{\partial}{\partial x}, \frac{\partial}{\partial y} = O(1), \quad w = O(\delta), \quad \frac{\partial}{\partial z} = O(\delta^{-1}). \tag{2.21}$$

On comparison of (2.18), (2.19) with (2.20), (2.21) it is found that the only estimate for ϕ and ψ that is consistent with *both* (2.20) and (2.21) is

$$\phi = O(\delta^2), \quad \psi = O(\delta), \tag{2.22}$$

and consequently, if y is the normal coordinate then

$$v_\phi, v_\psi = O(\delta), \quad w_\phi = O(\delta^2), \quad w_\psi = O(1), \tag{2.23}$$

and if z is the normal coordinate then

$$w_\phi, w_\psi = O(\delta), \quad v_\phi = O(\delta^2), \quad v_\psi = O(1). \tag{2.24}$$

It follows that an assumption

$$|\boldsymbol{U}_\phi| = O(\delta), \quad u, |\boldsymbol{U}_\psi| = O(1) \tag{2.25}$$

is required by boundary-layer scalings in which *either* of the transverse coordinates y or z can be taken as the normal coordinate. Note that as a consequence of (2.23) and (2.24), the composite velocity components v and w are both $O(1)$, and thus these scalings for $\boldsymbol{U}_\phi$ and $\boldsymbol{U}_\psi$ are compatible with a rotational inviscid flow in the corner region and elsewhere outside the viscous layer, in which v and w are of order unity.

It is of further interest to estimate the magnitudes of ϕ and ψ likely to occur in the cross-section outside the inner viscous region. Equations governing ϕ and ψ will later be derived by combining (2.11) with the continuity equation and the definition of streamwise vorticity Ω_1. These equations have the form of a 'Poisson' equation in the transverse coordinates, and defining $\delta u \equiv u - U$, it is easily shown that the forcing functions are $\partial(\delta u)/\partial x$ for the equation governing ϕ, and Ω_1 for the equation governing ψ. Assuming that the normal components of $\boldsymbol{U}_\phi$ and $\boldsymbol{U}_\psi$ are zero on boundaries, ϕ and ψ are essentially integrals of these forcing functions, and thus estimates of the prevailing order of magnitude of ϕ and ψ can be obtained by estimating $\partial(\delta u)/\partial x$ and Ω_1 respectively.

The potential-core region should behave in a manner analogous to the straight duct, and the quantity δu thus represents the displacement effect of the shear layers on the interior flow (blockage). If δ^* is taken to represent the 'average' displacement thickness for the cross-section, and if U and the cross-sectional area are taken as 1, then δu is related to δ^* by

$$1 + \delta u = (1 - \delta^*)^{-1} = 1 + \delta^* + O(\delta^{*2}). \tag{2.26}$$

Since $\partial/\partial x = O(1)$, it follows that $\partial(\delta u)/\partial x$ and ultimately $\boldsymbol{U}_\phi$ are of order δ^* for the displacement-interaction effect.

When the largest source of streamwise vorticity present is that generated in the outer portion of the boundary layer by turning, Ω_1 can be estimated from the Squire–Winter formula of secondary-flow theory (cf. Horlock & Lakshminarayana 1973*a*), which can be written as

$$\Delta\Omega_1 = -2\int \frac{\eta}{R}\,\mathrm{d}x. \tag{2.27}$$

Here $\Delta\Omega_1$ is the change in Ω_1 along a streamline whose principal radius of curvature is R, and η is transverse vorticity in the direction of R. Since η is of order δ^{-1} in the

boundary layer, the increase in Ω_1 will surpass the $O(\delta^*)$ level of $\partial(\delta u)/\partial x$ in a very short axial distance, and thus $\boldsymbol{U}_\psi$ will become large relative to $\boldsymbol{U}_\phi$, unless R is very large. As pointed out in § 1, the change in Ω_1 is 50 % of η after a deflection angle $\mathrm{d}x/R$ of only 15°. The large secondary velocity $\boldsymbol{U}_\psi$ will convect Ω_1 into the flow field and distort contours of the primary velocity u. Although the distortion of u eventually contributes to δu, this effect *follows* the generation of large $\boldsymbol{U}_\psi$ and occurs where $\boldsymbol{U}_\psi$ is already large. In light of these observations, it is concluded that an assumption such as (2.25) is reasonable throughout the cross-section.

Finally, if the flow is incompressible, it can become fully developed ($\partial/\partial x \equiv 0$). Since $\partial(\delta u)/\partial x$ is zero in a fully developed flow region, and since the normal component $\boldsymbol{U}_\phi$ is zero on boundaries, it follows that $\boldsymbol{U}_\phi$ is identically zero in a fully developed flow. As a consequence all approximations based on an assumption of small $\boldsymbol{U}_\phi$ become exact in regions of fully developed flow. It is also worth noting that if the x-coordinate is not aligned with the given potential flow (V, $W \neq 0$) then the present formulation does not necessarily require that V and W be small; it is only necessary that the corrections v_ϕ and w_ϕ are small.

2.5. *Inviscid approximations for convective terms*

For convenience in defining the present approximations, a parameter β (to be assigned a value of 0 or 1) is introduced in the expressions for transverse velocity components as follows;

$$v = V + v_\phi + v_\psi, \qquad \tilde{v} = V + \beta v_\phi + v_\psi, \tag{2.28}$$

$$w = W + w_\phi + w_\psi, \quad \tilde{w} = W + \beta w_\phi + w_\psi. \tag{2.29}$$

The approximation to be defined by choosing $\beta = 0$ will be referred to here as the small-scalar-potential approximation. Using (2.28) and (2.29), the components of the convective term $\boldsymbol{C}(\boldsymbol{U}) \equiv (\boldsymbol{U}\cdot\boldsymbol{\nabla})\,\boldsymbol{U}$ can be expressed in orthogonal coordinates as follows:

$$C_1 = \boldsymbol{U}\cdot\boldsymbol{\nabla}u + u(vK_{12} + wK_{13}) - v^2K_{21} - w^2K_{31}, \tag{2.30}$$

$$\tilde{C}_2 = \boldsymbol{U}\cdot\boldsymbol{\nabla}\tilde{v} - u(uK_{12} - \tilde{v}K_{21}) - w(\tilde{w}K_{32} - \tilde{v}K_{23}), \tag{2.31}$$

$$\tilde{C}_3 = \boldsymbol{U}\cdot\boldsymbol{\nabla}\tilde{w} - u(uK_{13} - \tilde{w}K_{31}) + v(\tilde{w}K_{32} - \tilde{v}K_{23}), \tag{2.32}$$

where the quantities K_{ij} are the geodesic curvatures of the coordinates, defined by

$$K_{ij} \equiv (h_i h_j)^{-1}\frac{\partial h_i}{\partial x_j}, \tag{2.33}$$

and in which x_1, x_2, x_3 are interchangeable with x, y, z respectively. The present convective approximation is made by setting $\beta = 0$ in (2.28) and (2.29) and hence in $\tilde{C}_2, \tilde{C}_3$; no approximation is made in C_1. If $\beta = 1$, then $\tilde{v}, \tilde{w} = v, w$, and the above expressions for $\tilde{C}_2$, $\tilde{C}_3$ revert to C_2, C_3, their exact forms.

The particular form of the approximations (2.31) and (2.32) in transverse convective terms entails the following considerations.

From the order-of-magnitude estimates of (2.20) and (2.21), it is evident that all terms of the convective operator

$$\boldsymbol{U}\cdot\boldsymbol{\nabla} = \frac{u}{h_1}\frac{\partial}{\partial x} + \frac{v}{h_2}\frac{\partial}{\partial y} + \frac{w}{h_3}\frac{\partial}{\partial z} \tag{2.34}$$

must be retained, since each term is $O(1)$ when either y or z is the normal coordinate. Since $\boldsymbol{U}\cdot\boldsymbol{\nabla}$ is an $O(1)$ operator, when it is applied to the transverse velocity components v_ϕ, w_ϕ, v_ψ, w_ψ the resulting convective terms are the same order as the velocity

components themselves, as given in (2.23) and (2.24). As a consequence, setting $\beta = 0$ retains all $O(1)$ terms and neglects only $O(\delta)$ terms containing v_ϕ, w_ϕ. All remaining terms in (2.31) and (2.32) are curvature terms containing K_{ij}; these are assumed to be $O(1)$ terms and are retained. The curvature terms do not affect the analysis of characteristics, and the only purpose for approximating these terms as shown in (2.31) and (2.32) is that some simplification will occur when the equations are later reformulated for numerical solution. All of the approximations in (2.31) and (2.32) are consistent with the assumption of small $\boldsymbol{U}_\phi$ as in (2.25).

Viscous approximations will be introduced in §2.6. If the modified viscous force is denoted by $\boldsymbol{F}'$, then the momentum equations as approximated here can be expressed as $\rho \boldsymbol{M} = 0$, where the components of $\boldsymbol{M}$ are given by

$$M_1 = C_1 + (\rho h_1)^{-1} \frac{\partial p}{\partial x} - Re^{-1} F_1' = 0, \tag{2.35}$$

$$M_2 = \tilde{C}_2 + (\rho h_2)^{-1} \frac{\partial p}{\partial y} - Re^{-1} F_2' = 0, \tag{2.36}$$

$$M_3 = \tilde{C}_3 + (\rho h_3)^{-1} \frac{\partial p}{\partial z} - Re^{-1} F_3' = 0. \tag{2.37}$$

Note that no approximation has been made in the streamwise convective term C_1 or in any pressure gradient term in (2.35)–(2.37). The continuity equation remains unapproximated as in (2.1).

2.6. *Viscous approximation neglecting streamwise diffusion*

The viscous force $\boldsymbol{F}$ in (2.2) can be written for constant μ as

$$\rho \boldsymbol{F} = -\mu \nabla \times \boldsymbol{\Omega} + (\lambda + 2\mu) \nabla (\nabla \cdot \boldsymbol{U}), \tag{2.38}$$

where $\boldsymbol{\Omega} \equiv \nabla \times \boldsymbol{U}$ is vorticity and μ and λ are viscosity coefficients. The boundary layer order-of-magnitude estimates of (2.20)–(2.24), supplemented by $Re = O(\delta^{-2})$, are employed to estimate the importance of viscous terms. It is found that all terms that contain either a derivative with respect to x or that contain v_ϕ or w_ϕ are $O(\delta)$ or smaller, and this justifies neglecting any such term. Although some other $O(\delta)$ terms are present which might be neglected, if only terms containing $\partial/\partial x$, v_ϕ or w_ϕ are neglected, then the approximation will have the desirable attribute of being exact for a fully-developed incompressible flow (recall that $\boldsymbol{U}_\phi = 0$ in this case).

For moderate subsonic Mach numbers $\nabla \cdot \boldsymbol{U}$ is small, and thus the last term in (2.38) is neglected here. Neglecting all x-derivatives gives the following approximation for F_1' in orthogonal coordinates:

$$(h_1 h_2 h_3) \rho F_1' = \mu \left[\frac{\partial}{\partial y} \frac{h_1^2 h_3}{h_2} \frac{\partial}{\partial y} \left(\frac{u}{h_1} \right) + h_1^2 h_3 K_{12} \frac{\partial}{\partial y} \left(\frac{u}{h_1} \right) + \frac{\partial}{\partial z} \frac{h_1^2 h_2}{h_3} \frac{\partial}{\partial z} \left(\frac{u}{h_1} \right) + h_1^2 h_2 K_{13} \frac{\partial}{\partial z} \left(\frac{u}{h_1} \right) \right]. \tag{2.39}$$

By neglecting x-derivatives in the transverse components of $\nabla \times \boldsymbol{\Omega}$, the viscous terms F_2' and F_3' can be approximated in terms of the streamwise vorticity Ω_1 as follows:

$$(h_1 h_3) \rho F_2' = -\frac{\mu \partial (h_1 \Omega_1)}{\partial z}, \tag{2.40}$$

$$(h_1 h_2) \rho F_3' = \frac{\mu \partial (h_1 \Omega_1)}{\partial y}, \tag{2.41}$$

where

$$\Omega_1 = (h_2 h_3)^{-1}\left[\frac{\partial(h_3 w_\psi)}{\partial y} - \frac{\partial(h_2 v_\psi)}{\partial z}\right]. \tag{2.42}$$

Note that none of the viscous terms remaining in (2.40)–(2.42) depend on U_ϕ, and thus the present approximation neglecting streamwise diffusion differs from that conventionally adopted by neglecting all x-derivatives of u, v and w. Subsequently, the difference between these two methods of approximating viscous terms in the transverse momentum equations will be shown to affect the classification of the system of equations.

2.7. *Approximations affecting total enthalpy*

For compressible flow a second inviscid approximation is made, neglecting U_ϕ in the definition (2.4) of stagnation enthalpy as follows:

$$E \approx \tilde{E} \equiv T + \tfrac{1}{2}(\gamma - 1) M_r^2 \tilde{q}^2, \tag{2.43}$$

where $\tilde{q}^2 \equiv u^2 + \tilde{v}^2 + \tilde{w}^2$. As before, if $\beta = 1$ then $\tilde{E} = E$, and the above expression reverts to its exact form. The state equation (2.6) now becomes

$$p = \frac{\rho \tilde{E}}{\gamma M_r^2} - \frac{(\gamma - 1)\rho \tilde{q}^2}{2\gamma}. \tag{2.44}$$

If the stagnation enthalpy is not constant, an energy equation is solved. In the energy equation (2.5) the bracketed terms are small for moderate subsonic Mach numbers and especially if $Pr \approx 1$. Neglecting these terms, setting $E \approx \tilde{E}$, and neglecting all conduction terms containing an x-derivative, the energy equation can be approximated as

$$\rho \boldsymbol{U} \cdot \boldsymbol{\nabla} \tilde{E} = (Re\, Pr)^{-1} \boldsymbol{\nabla} \cdot k \boldsymbol{\nabla}_s \tilde{E}. \tag{2.45}$$

An approximate form of (2.5) which includes some of the terms in brackets is given in Appendix B.

2.8. *Summary of approximating equations*

For compressible flow, the small-scalar-potential approximation provides a system of eight equations governing the five velocity components u, v_ϕ, w_ϕ, v_ψ, w_ψ, pressure p, density ρ and modified total enthalpy $\tilde{E}$. The equations consist of continuity (2.1), three components of momentum (2.35)–(2.37), the state equation in the form (2.44), the energy equation (2.45), and the decomposition identities (2.15) and (2.16). These latter identities are needed because of the increase in the number of dependent variables which occurs as a result of the velocity decomposition. For an incompressible flow ρ and $\tilde{E}$ are constants, and the state and energy equations are omitted.

Although the dependent variables given above are convenient for the analysis of characteristics in §3, they are not convenient for numerical solution, and for this purpose the equations are reformulated in terms of the axial velocity u, pressure p, streamwise vorticity Ω_1, scalar and vector surface potentials ϕ and ψ, together with density ρ and modified total enthalpy $\tilde{E}$. Second-order equations for Ω_1 and p are derived by taking the divergence and curl of the transverse vector momentum equation. These two second-order equations then replace the two transverse momentum equations and the two first-order decomposition identities. Letting $\boldsymbol{M}_s \equiv \boldsymbol{i}_2 M_2 + \boldsymbol{i}_3 M_3$ denote the vector transverse momentum equation including all

approximations, the equations governing streamwise vorticity Ω_1 and pressure p are given by

$$\boldsymbol{i}_1 \cdot \boldsymbol{\nabla} \times \rho \boldsymbol{M}_s = 0, \tag{2.46}$$

$$\boldsymbol{\nabla} \cdot \rho \boldsymbol{M}_s = 0. \tag{2.47}$$

Incorporating the definitions of $\boldsymbol{U}_\phi$ and $\boldsymbol{U}_\psi$, the continuity equations becomes

$$\boldsymbol{\nabla} \cdot \rho(\boldsymbol{i}_1 u + \boldsymbol{\nabla}_s \phi + \boldsymbol{U}_s) = 0, \tag{2.48}$$

and the definition of Ω_1 becomes

$$\Omega_1 = \boldsymbol{i}_1 \cdot \boldsymbol{\nabla} \times [\rho^{-1} \boldsymbol{\nabla} \times \boldsymbol{i}_1 \psi + \boldsymbol{U}_s]. \tag{2.49}$$

The final system of equations consists of (2.46)–(2.49) above, the x-momentum equation (2.35), the state equation (2.44) and the energy equation (2.45). These equations are given for a general orthogonal coordinate system in Appendix B.

3. Suitability for forward-marching solution

3.1. *Classification of equations*

Systems of partial differential equations have been classified as elliptic, hyperbolic or parabolic according to the roots of the characteristic polynomial equation (e.g. Courant & Hilbert 1966). Systems of an intermediate type which do not fit any one of these categories are encountered here and elsewhere. The present concern, however, is only whether the equations permit or preclude solution as a well-posed initial/boundary-value problem, by integration in a 'time-like' coordinate direction. Garabedian (1964) considers when an independent variable may be identified as a time-like variable, and citing an example problem for a linear homogeneous system with constant coefficients, concludes that it is natural to require that every root of the characteristic equation be real, as this excludes solutions that may grow exponentially with the time-like variable. This criterion is employed here to test systems of equations for time-like behaviour in a chosen coordinate variable. In view of the exponential growth which may occur in linear systems with constant coefficients, systems with one or more imaginary roots are presumed to be ill-posed for solution as an initial/boundary-value problem and are referred to here as elliptic (with respect to the chosen coordinate). Systems with no imaginary root for the time-like coordinate are presumed to be well-posed and are referred to as non-elliptic.

The present system of equations is of mixed order in that the velocity components appear in second-order derivatives, while the pressure appears only in first-order terms. To classify this mixed-order system, it is first rewritten as an equivalent first-order system and then examined following standard procedures for classification of n-dimensional systems of first-order partial differential equations (e.g. Courant & Hilbert 1966). The equations can be written as the following quasilinear system of m three-dimensional partial differential equations:

$$\boldsymbol{A}_1 \frac{\partial \boldsymbol{\Phi}}{\partial x} + \boldsymbol{A}_2 \frac{\partial \boldsymbol{\Phi}}{\partial y} + \boldsymbol{A}_3 \frac{\partial \boldsymbol{\Phi}}{\partial z} = \boldsymbol{B} \tag{3.1}$$

for the m-dimensional column vector $\boldsymbol{\Phi}$ of dependent variables, and with x, y, and z the independent variables (spatial coordinates). The square matrices $\boldsymbol{A}_i$ and the column vector $\boldsymbol{B}$ contain coefficients depending only on x, y, z and $\boldsymbol{\Phi}$. The derivative

operators $\partial/\partial x$, $\partial/\partial y$, $\partial/\partial z$ are replaced by λ_x, λ_y and λ_z respectively, and the mth-order characteristic polynomial equation is given by the determinant

$$|\boldsymbol{A}_1\lambda_x+\boldsymbol{A}_2\lambda_y+\boldsymbol{A}_3\lambda_z| = 0. \tag{3.2}$$

Since x has been identified here as the time-like coordinate, it is appropriate to examine (3.2) for imaginary roots λ_x, assuming that arbitrary real values are assigned for λ_y, λ_z.

Since the viscous terms will be small over much of the flow region, the approximating equations must be non-elliptic both with viscous terms present and in the inviscid limit of small viscosity. The presence of second-order viscous terms suppresses the influence of first-order terms on the characteristic equation (selectively if the system is of mixed order). Since all second-order terms disappear in the limit of small viscosity, the viscous characteristic equation is degenerate in this limit, and consequently, the viscous and inviscid cases must be considered separately.

3.2. *The viscous characteristic equation*

Only the incompressible form of the viscous equations is considered here. Since coordinate curvature terms do not affect the characteristic equation, it is sufficient to consider the Cartesian form of the equations. Taking $\rho = \tilde{E} = \mu = 1$ and $\boldsymbol{U}_s = 0$, the equations assume a particularly simple form which clarifies how the small scalar-potential approximation appears in the equations. Introducing new variables F and G as needed for second-order terms, these equations can be expressed as the following first-order system:

$$\frac{\partial u}{\partial x}+\frac{\partial v_\phi}{\partial y}+\frac{\partial w_\phi}{\partial z} = 0, \tag{3.3}$$

$$(\boldsymbol{U}\cdot\boldsymbol{\nabla})\,u+\frac{\partial p}{\partial x} = Re^{-1}\left(\frac{\partial F}{\partial y}+\frac{\partial G}{\partial z}\right), \tag{3.4}$$

$$(\boldsymbol{U}\cdot\boldsymbol{\nabla})\,(\beta v_\phi+v_\psi)+\frac{\partial p}{\partial y} = -Re^{-1}\frac{\partial \boldsymbol{\Omega}_1}{\partial z}, \tag{3.5}$$

$$(\boldsymbol{U}\cdot\boldsymbol{\nabla})\,(\beta w_\phi+w_\psi)+\frac{\partial p}{\partial z} = Re^{-1}\frac{\partial \boldsymbol{\Omega}_1}{\partial y}, \tag{3.6}$$

$$\frac{\partial v_\phi}{\partial z}-\frac{\partial w_\phi}{\partial y} = 0, \tag{3.7}$$

$$\frac{\partial v_\psi}{\partial y}+\frac{\partial w_\psi}{\partial z} = 0, \tag{3.8}$$

$$\frac{\partial v_\psi}{\partial z}-\frac{\partial w_\psi}{\partial y} = \boldsymbol{\Omega}_1, \tag{3.9}$$

$$\frac{\partial F}{\partial z}-\frac{\partial G}{\partial y} = 0, \tag{3.10}$$

$$F \equiv \frac{\partial u}{\partial y} \quad \text{or} \quad G \equiv \frac{\partial u}{\partial z}. \tag{3.11a,b}$$

The characteristic equation for the system (3.3)–(3.11a) is given by

$$Re^{-2}\lambda_y(\lambda_y^2+\lambda_z^2)^4 = 0 \tag{3.12}$$

Since (3.12) has no imaginary roots in λ_x, the viscous equations in the form given here are non-elliptic. In fact, since λ_x does not appear in (3.12), this system is parabolic. Furthermore, the parameter β does not appear in (3.12), and thus the viscous approximation used here produces nonelliptic equations even if the inviscid approximation $\beta = 0$ is not made. Other methods of neglecting streamwise diffusion may not lead to nonelliptic equations. In Appendix A it is shown that the conventional method which neglects all x-derivatives of u, v and w produces an elliptic system unless inviscid terms are also approximated. Even though the present viscous system of equations is parabolic, however, the viscous characteristic equation (3.12) is degenerate as $Re^{-2} \to 0$, and as mentioned previously, the characteristic equation for the inviscid system must also be considered for regions of inviscid flow.

3.3. *The inviscid characteristic equation*

The incompressible Euler equations are given by (3.3)–(3.8) with $Re^{-1} = 0$. The characteristic equation for this system is

$$(u\lambda_x + v\lambda_y + w\lambda_z)^2 (\lambda_y^2 + \lambda_z^2)(\beta\lambda_x^2 + \lambda_y^2 + \lambda_z^2) = 0. \tag{3.13}$$

The three factors in (3.13) are respectively of hyperbolic, parabolic and elliptic form. For the Euler equations ($\beta = 1$) there is one pair of imaginary roots λ_x associated with the last factor. The well-known result that the incompressible Euler equations are elliptic follows from the occurrence of imaginary roots in (3.13). When the small-scalar-potential approximation is made ($\beta = 0$), the imaginary roots associated with the last factor in (3.13) are removed, and thus this approximation produces a non-elliptic approximation of the incompressible Euler equations.

The compressible Euler equations are given by (2.1), (2.15), (2.16), (2.35)–(2.37), (2.44) and (2.45), with $Re^{-1} = 0$, and the characteristic equation for this system is given by

$$(u\lambda_x + v\lambda_y + w\lambda_z)^3 (\lambda_y^2 + \lambda_z^2)[(\beta\lambda_x^2 + \lambda_y^2 + \lambda_z^2) - M_r^2 T^{-1}(u\lambda_x + a_1)(\beta u\lambda_x + a_2)] = 0, \tag{3.14}$$

where

$$a_1 = [\gamma v + (1-\gamma)\tilde{v}]\lambda_y + [\gamma w + (1-\gamma)\tilde{w}]\lambda_z, \tag{3.15}$$

$$a_2 = (\beta V + \tilde{v})\lambda_y + (\beta W + \tilde{w})\lambda_z. \tag{3.16}$$

For $\beta = 1$ the bracketed term in (3.14) has one pair of imaginary roots for sufficiently small values of the Mach number M_r, and in this case the equations are elliptic. For $\beta = 0$ this bracketed term is a first-order polynomial in λ_x, and as such can have no imaginary roots. Consequently the small scalar-potential approximation ($\beta = 0$) produces a non-elliptic approximation for the compressible Euler equations, for any value of Mach number.

For the special case in which all components of the transverse velocity are zero, then $a_1 = a_2 = 0$, and if the local Mach number defined by $M^2 \equiv M_r^2 u^2/T$ is introduced then the bracketed term in (3.14) becomes

$$[\beta(1 - M^2)\lambda_x^2 + \lambda_y^2 + \lambda_z^2], \tag{3.17}$$

which reproduces the well-known result that the Euler equations ($\beta = 1$) are elliptic for $M < 1$.

4. Numerical solution procedure

4.1. *Differencing procedures and boundary conditions*

Streamwise derivative terms in the governing equations have a form such as $u\partial(\ )/\partial x$, and because the streamwise velocity u is very small in the viscous-dominated region near no-slip walls, it is essential to use implicit algorithms which are not subject to stringent stability restrictions unrelated to accuracy requirements. The present method is semi-implicit and seeks to reduce the amount of iteration and other computational labour required and yet avoid the more severe stability restrictions of explicit algorithms. In all of the calculations performed here and elsewhere while developing the solution algorithm, the streamwise step size has been limited only by accuracy considerations and not by instability. The present method of solution is also very economical, considering the general complexity of the system of governing equations. The algorithm can be coded such that an entire three-dimensional flowfield requires roughly the same computational labour as one or two time-step iterations of an efficient implicit algorithm for the compressible Navier–Stokes equations (e.g. Briley & McDonald 1977), assuming the same grid is used. Since time-iterative algorithms for the Navier–Stokes equations presently require a minimum of 50–100 time-step iterations to compute a steady solution, the present method is well over 10 times more economical and also requires far less computer storage. The run time is in the range of 0.006–0.036 s per grid point (CDC 7600).

The governing equations are replaced by an implicit finite-difference approximation whose formal accuracy is $O(\Delta x, \Delta y^2, \Delta z^2)$. The algorithm employs two-point backward differences for streamwise (x) derivatives and three-point central differences for transverse (y or z) derivatives. The streamwise step size Δx is variable, and an analytical coordinate transformation devised by Roberts (1971) is employed for each transverse coordinate direction, as a means of introducing a non-uniform grid to concentrate grid points in the wall shear-layer regions. Although a centred Crank–Nicolson formulation could be used for axial derivatives, the formal accuracy would not be improved in the present algorithm, since 'nonlinear coefficients' which depend on certain dependent variables are evaluated explicitly during portions of the solution procedure. The explicit evaluation of these nonlinear coefficients serves to linearize and decouple selected equations and variables from the remaining equations and variables, and this both simplifies and provides economy in the solution procedure. Second-order accuracy is rigorously maintained for the transverse coordinate directions. No 'upwinding' or artificial dissipation of any kind is used for the transverse coordinate directions.

In all of the solutions reported here, no-slip or symmetry boundary conditions are prescribed, as appropriate, and the adiabatic wall condition $\partial\tilde{E}/\partial n = 0$ was used, where n denotes the surface normal coordinate. No boundary condition is required for density, since it is computed algebraically from the state equation. The no-slip condition $v = w = 0$ must be expressed in terms of ϕ, ψ and Ω_1. The normal velocity component is specified by prescribing $\psi = 0$ and the Neumann condition $\partial\phi/\partial n = 0$. The tangential component of the no-slip condition is written as

$$\boldsymbol{i}_t \cdot [\boldsymbol{U}_s + \boldsymbol{\nabla}_s \phi + \rho^{-1} \boldsymbol{\nabla} \times \boldsymbol{i}_1 \psi] = 0, \tag{4.1}$$

where $\boldsymbol{i}_t$ denotes the unit tangent vector, and the finite-difference forms of (2.49) and (4.1) are combined to provide a boundary condition relating Ω_1 at the wall to ϕ and

ψ. A Neumann boundary condition for pressure p at a no-slip wall is obtained from the normal momentum equation as

$$\boldsymbol{i}_n \cdot [\nabla p - Re^{-1} \rho \boldsymbol{F}'] = 0, \tag{4.2}$$

where the convective terms vanish because $\boldsymbol{U} = 0$.

4.2. *Sequence of solution*

With the exception of the equations governing the streamwise vorticity Ω_1 and secondary-flow stream function ψ, the system of equations is decoupled here to allow each equation to be solved separately as a scalar equation. This requires a sequence of solution such that implicit variables not associated with the scalar equation currently being solved are available from solution of a previous scalar equation in the sequence. The equations governing streamwise vorticity and secondary-flow stream function are solved as a (linear) coupled system because the no-slip boundary conditions couple these equations in a way that would severely restrict the axial step size if these equations were treated as decoupled. An analogous situation is well known in time-dependent algorithms for the vorticity/stream-function form of the two-dimensional Navier–Stokes equations. The step-size limitation is much more severe in the present case because the 'time-like' derivatives have the form $u\partial(\ )/\partial x$, and $u \to 0$ at a no-slip wall.

In most applications, knowledge of initial (starting) conditions will be incomplete. Initial conditions must then be specified from a parametric or some other convenient description of the flow and then adjusted as part of a starting procedure to achieve a degree of local compatibility with the governing equations. A procedure for initializing and starting the algorithm will be outlined following a description of the algorithm itself. It is beneficial to introduce a further change of variables expressing the pressure p as a correction δp to the potential flow pressure P:

$$p = P + \delta p. \tag{4.3}$$

This will prove convenient in starting the algorithm when the given potential flow has nonzero streamwise pressure gradients ($\partial P/\partial x \neq 0$). Once the algorithm has been started, however, the continued use of (4.3) is a simple change of dependent variables and does not represent a physical approximation. The manner in which δp appears in the governing equations is unusual in that $\partial(\delta p)/\partial x$ appears only in the x-momentum equation and not in the pressure equation (2.47). It is thus beneficial to rewrite δp in the following form:

$$\delta p = p_m(x) + \Delta p(x, y, z), \tag{4.4}$$

where $\int A\,(\Delta p)\,\mathrm{d}A = 0$ for all x, and A denotes cross-sectional area. Equation (2.47) now governs Δp but does not contain p_m, which is in effect the arbitrary constant of the Neumann problem for Δp at each x-location. As a consequence, (2.47) can be solved for Δp *before* p_m is known, and p_m can then be adjusted during solution of the x-momentum equation (2.35) to ensure that the integral mass-flux relation

$$\int_A (\rho u)\,\mathrm{d}A = Q = \text{constant} \tag{4.5}$$

is satisfied.

A summary of the procedure used to advance the solution a single streamwise step to the $(n+1)$-level x^{n+1} from known quantities at x^n follows. Unless specifically mentioned to the contrary, the transverse velocities v_ϕ, w_ϕ, v_ψ, w_ψ and the density

ρ are evaluated explicitly at the n-level. In addition, the convective operator is evaluated as $\rho^n \boldsymbol{U}^n \cdot \boldsymbol{\nabla}$. Values of V, W, P, h_1, h_2 and h_3 are given and thus known at both x^n and x^{n+1}.

(1) Equations (B 1) and (B 2) form a linear coupled system for Ω_1^{n+1} and ψ^{n+1} which is solved as a 2×2 coupled system. For this purpose artificial time derivatives are added to each equation, and an iterative block-implicit scheme (Briley & McDonald 1980) is used. In prescribing no-slip boundary conditions, the tangential component (4.1) contains a contribution from ϕ; this contribution is evaluated using ϕ^n. Terms in the vorticity equation (B 1) containing u, v_ψ and w_ψ are evaluated using u^n, v_ψ^n and w_ψ^n; x-derivatives of v_ψ and w_ψ are evaluated using n- and $(n-1)$-level quantities.

(2) The pressure equation (B 3) is solved for Δp^{n+1} using an iterative scalar ADI scheme. In this equation all appearances of v_ψ^{n+1} and w_ψ^{n+1} are evaluated using ψ^{n+1}, and u, ρ, v_ϕ and w_ϕ are evaluated using n-level quantities.

(3) The energy equation (B 4) is solved for $\tilde{E}^{n+1}$ using a scalar ADI scheme.

(4a) Using an assumed value of p_{m}^{n+1} to begin a secant iteration, and values of Δp^n and Δp^{n+1} now available, the x-momentum equation (B 5) is solved to determine u^{n+1}, using a scalar ADI scheme.

(4b) The density ρ^{n+1} is evaluated algebraically from the state equation (B 6) using $\tilde{q}^{n+1}$, $\tilde{E}^{n+1}$, p_{m}^{n+1} and Δp^{n+1}, which are now available.

(4c) For internal flows the integral mass-flux relation (4.4) is evaluated using u^{n+1} and ρ^{n+1}.

(4d) Assuming that the initial guess for p_{m}^{n+1} was not exact, the integral mass-flux relation will not be satisfied, and steps (4a–c) are repeated iteratively using the standard secant method (cf. Ralston 1965) to find the value of p_{m}^{n+1} that leads to u^{n+1} and ρ^{n+1} satisfying the integral mass-flux relation (4.4). In the incompressible limit, all equations in this iteration are linear, and the secant iteration is exact on the third iteration. At high subsonic Mach numbers, a fourth or even fifth iteration may be required.

(5) Finally, the continuity equation (B 7) is solved for ϕ^{n+1} using an iterative scalar *ADI* scheme and currently available values of u^{n+1} and ρ^{n+1}. The velocity components v^{n+1}, w^{n+1}, $\tilde{v}^{n+1}$ and $\tilde{w}^{n+1}$ are then evaluated from ϕ^{n+1} and ψ^{n+1}.

4.3. *Starting Procedure*

Initial conditions for velocity are devised from the potential flow as follows:

$$(u, v, w) = (U, V, W) f(y_{\mathrm{w}}/\delta). \tag{4.6}$$

Here f is a von Kármán polynomial velocity profile (zero pressure gradient), y_{w} is the distance to the nearest wall, and δ is a specified mean boundary-layer thickness. The profile shape f is scaled such that $f = u_{\mathrm{b}}$ for $y_{\mathrm{w}} \geqslant \delta$, where u_{b} is a constant that adjusts for internal flow blockage, giving a non-dimensional mass flux of unity. In all calculations performed here, the initial total enthalpy was taken as constant, and the initial streamwise vorticity was taken as zero unless otherwise stated.

Using Ω^n, (B 2) is first solved to obtain ψ^n, and then taking Δp as zero, steps (3)–(5) of the algorithm are solved to obtain ϕ^{n+1}. Taking ϕ^n as ϕ^{n+1}, v^n and w^n are recomputed from ϕ^n, ψ^n, V and W, and a profile adjustment is made as in (4.6) to satisfy the no-slip conditions. The streamwise vorticity Ω^n is then redefined using v^n and w^n. This procedure ensures that the initial conditions for all variables except Δp are reasonably compatible with the governing equations and boundary conditions. The first step is then divided into a number (say 10) of smaller steps, and is computed taking $\Delta p = 0$ in the streamwise momentum equation. This allows the effect of the

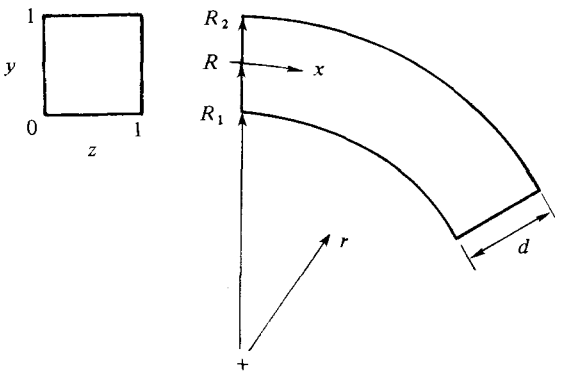

FIGURE 2. Geometry of circular-arc square duct.

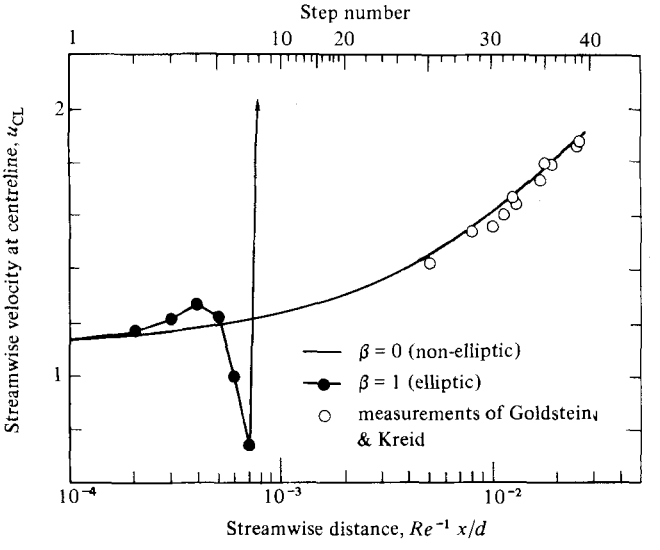

FIGURE 3. Effect of small-scalar-potential approximation on initial-value problem for a straight duct with $Re = 1000$, $\delta/d = 0.1$.

initial 'impulse' in streamwise gradients of v_ϕ, w_ϕ and hence Δp to decay before continuing, and is analogous to starting procedures for many boundary layer methods. The pressure correction Δp is then computed as in step (2) of the algorithm, and the calculation then proceeds using the complete algorithm. In some instances it has been found that introducing the streamwise pressure gradient term $\partial \Delta p/\partial x$ gradually over 5 or 10 streamwise steps eliminates streamwise oscillations.

5. Application to flow in a curved square duct

The analysis is applied to laminar subsonic flow in a circular-arc duct of square cross-section as shown in figure 2. A potential-flow coordinate system is used such that orthogonal streamlines and velocity potential lines from an incompressible potential flow form the axial and radial coordinates respectively, and the third coordinate consists of straight lines normal to the endwall planes. This coordinate

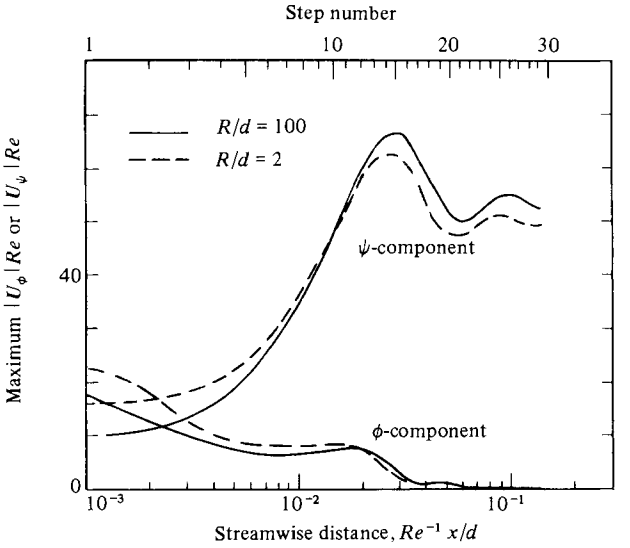

FIGURE 4. Validation of the small-scalar-potential approximation for flow in a circular-arc square duct with $K = 100$, $\delta/d = 0.1$.

system is defined by $h_1 = h_2 = r \ln (R_2/R_1)$ and $h_3 = 1$. This potential flow has an axial velocity U given by $U = r^{-1}/\ln (R_2/R_1)$, with $V = W = 0$ and $P = 1 - U^2$. Computed results are given for cases having both large and small curvature, and both thick and thin inlet shear layers. All flow cases considered here were computed for $M_r = 0.05$ and $P_r = 1$.

5.1. *Demonstration of a well-posed initial/boundary-value problem*

Before considering the flow in curved ducts, the role of the small-scalar-potential approximation in defining a well-posed initial/boundary-value problem was tested empirically in calculations for a straight duct with $Re = 1000$ (based on d) and with an inlet shear-layer thickness $\delta/d = 0.1$. Two calculations were performed, one with $\beta = 0$ and the other with $\beta = 1$; the calculations were otherwise identical in every detail. The streamwise development of centreline velocity from these calculations is shown in figure 3 with the customary scaling of streamwise distance. The elliptic case ($\beta = 1$) was found to display behaviour indicative of an ill-posed problem, whereas the non-elliptic case ($\beta = 0$) representing the small-scalar-potential approximation appears well-posed and also agrees with the measurements of Goldstein & Kreid (1967). All remaining calculations considered here were performed with $\beta = 0$.

5.2. *Validation of the small-scalar-potential approximation*

Calculations were performed for cases whose centreline radius of curvature R is both large ($R/d = 100$) and small ($R/d = 2$), each case having $\delta/d = 0.1$. The Dean number $K = Re\,(d/R)^{\frac{1}{2}}$ was fixed at 100 for each case, to facilitate comparison both between the two solutions and (for large x) with the recent calculations of Ghia *et al.* (1981) for the incompressible fully developed flow regime. The maximum absolute value of each (ϕ or ψ) component of transverse velocity is shown against streamwise distance in figure 4 for each case. For a given value of K, the scaling shown is known to remove much of the dependence on curvature. The results in figure 4 show that the ϕ-component of the transverse velocity U_s is significantly less than the ψ-component,

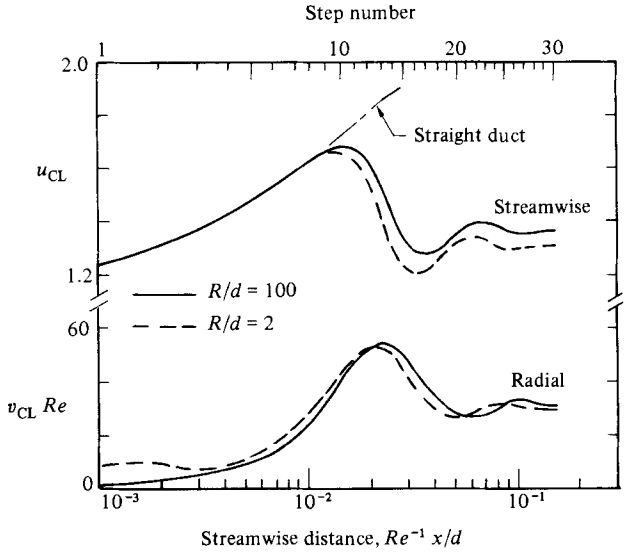

FIGURE 5. Streamwise (u) and radial (v) velocities at centreline for a circular-arc square duct with $K = 100$, $\delta/d = 0.1$.

except very near the start of the calculation. This comparison is taken as an indication that the assumption of small U_ϕ is valid in the developing-flow region where most practical applications occur, and for both large and small radius of curvature.

The behaviour of streamwise and radial centreline velocity against streamwise distance is shown in figure 5 for these two cases. The structure of these developing flows is such that the centreline streamwise velocity initially proceeds along the path followed in a straight duct; this reflects acceleration due to the viscous displacement (blockage) effect. The departure from this path (beginning around streamwise step number 10) represents distortion of the primary flow by the secondary flow, as evidenced by the large radial velocity at the centreline. The oscillatory behaviour with increasing x is consistent with Hawthorne's (1951) observation in inviscid secondary-flow theory that an oscillatory behaviour will occur once there is sufficient distortion of the primary flow. Finally, figure 5 shows that a slight dependence on R/d persists even in the fully developed regime.

Finally, it is noted that for the low Mach number considered ($M = 0.05$), there is a quasi-fully-developed flow region beginning around $(x/d)\,Re^{-1} = 10^{-1}$, where the compressible flow has essentially the same behaviour as in the asymptotic fully developed flow regime of an incompressible flow. In this quasi-fully-developed region the ϕ-component approaches zero (figure 4), and the small-scalar-potential approximation in fact reduces (in the incompressible limit) to the exact equations governing fully developed flow. Further downstream, the Mach number of a compressible flow will increase owing to viscous heating, and the flow will eventually choke. The accuracy of the present calculations can be examined in this quasi-fully-developed flow region by comparison with the recent calculations of Ghia *et al.* (1981). A representative comparison for both streamwise and radial velocity is shown in figures 6(a,b) for the case with $K = 100$, $R/d = 100$ and $Re = 1000$, and very good agreement is observed. The data points shown are representative of the Ghia *et al.* solution, but do not correspond to their grid points.

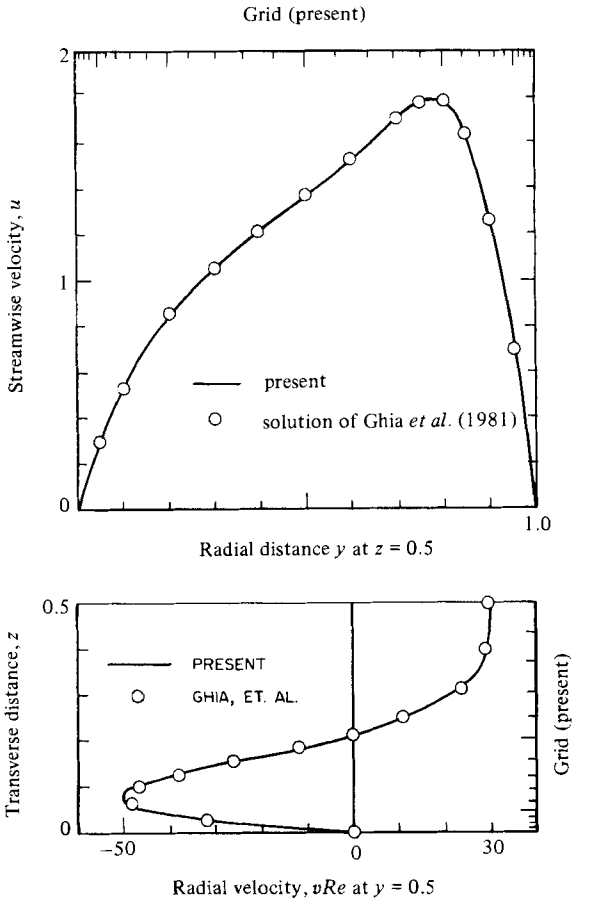

FIGURE 6. Fully developed flow with $K = 100$, $R/d = 100$, $Re = 1000$: (*a*) streamwise-velocity profile; (*b*) radial-velocity profile.

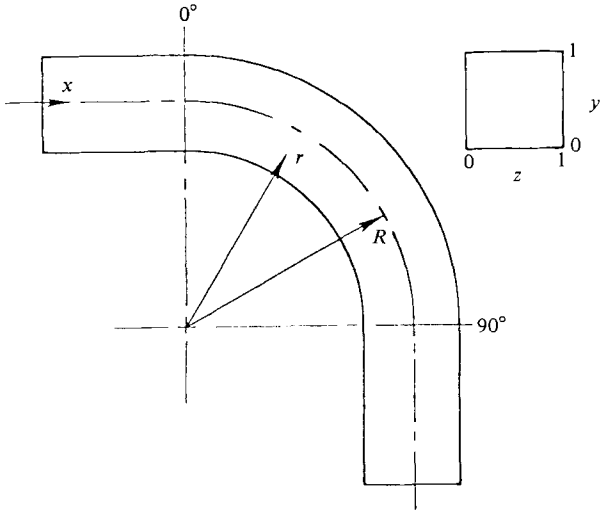

FIGURE 7. Geometry for 90° bend with $R/d = 2.3$.

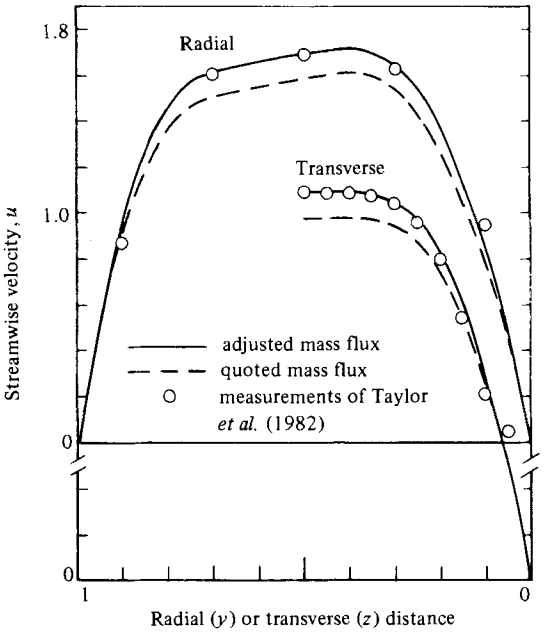

FIGURE 8. Comparison of initial conditions (0°) and measurements ($-0.5d$) for 90° bend with $R/d = 2.3$, $Re = 790$, $\delta/d = 0.4$.

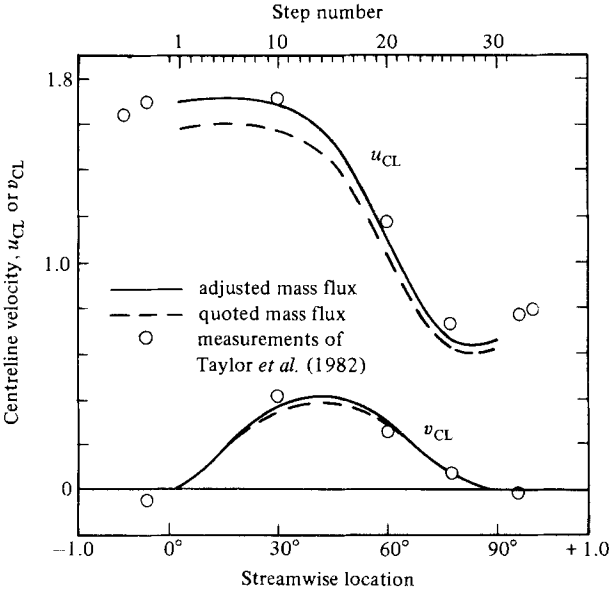

FIGURE 9. Streamwise (u) and radial (v) velocities at centreline for a 90° bend with $R/d = 2.3$, $Re = 790$, $\delta/d = 0.4$.

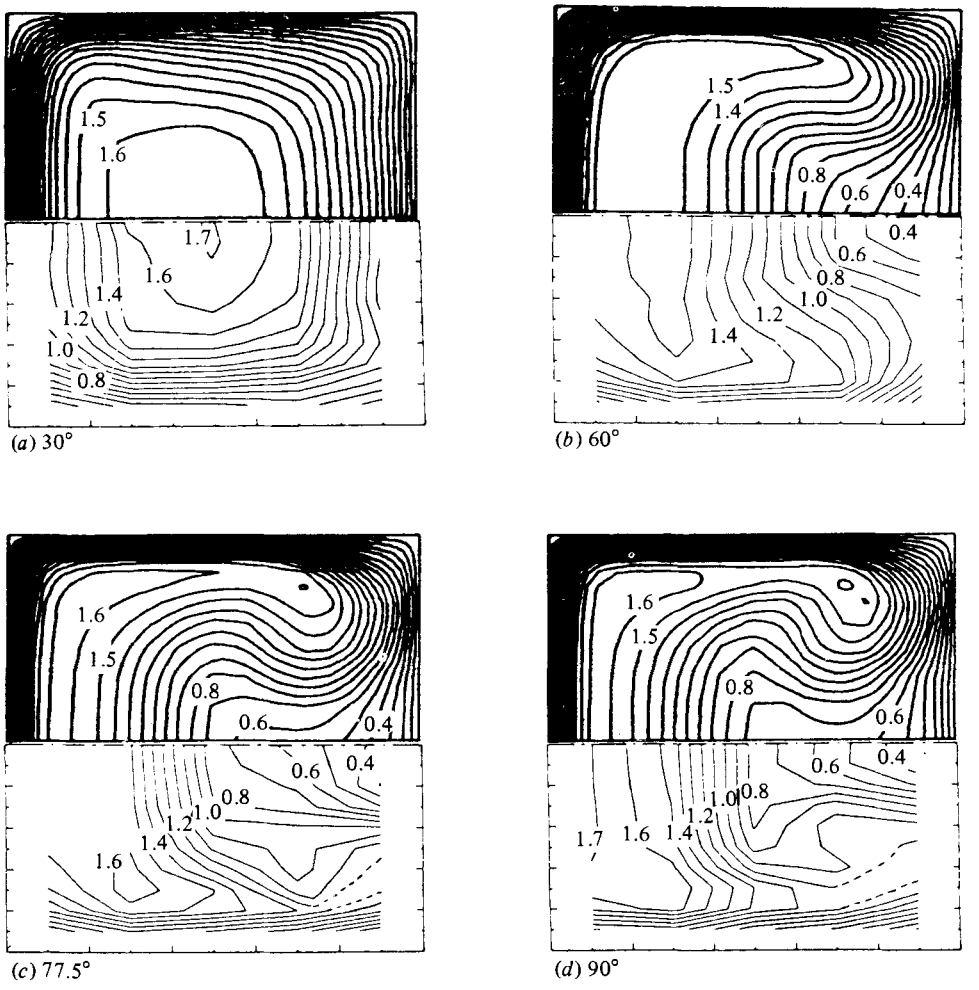

FIGURE 10. Computed (top) and measured (bottom) streamwise velocity contours for a 90° bend with $R/d = 2.3$, $Re = 790$, $\delta/d = 0.4$. Computed contours have adjusted mass flux (inside of bend is to right).

5.3. *Comparison with experimental measurements*

Taylor, Whitelaw & Yianneskis (1980) have obtained laser velocimetry measurements of both radial and streamwise velocity components in a 90° bend of square cross-section and curvature $R/d = 2.3$. Their measurements were taken for a Reynolds number $Re = 790$, and the inflow conditions correspond to a shear-layer thickness of approximately $\delta/d = 0.4$. The geometry is shown in figure 7 and includes straight extensions both upstream and downstream of the bend. The coordinate system in use here did not allow for computation in the straight extensions of the geometry, and thus the calculation was started at the start of the bend (0°). A 29 × 15 non-uniform grid was used for the (y, z) cross-section. Although a potential-flow code for this geometry was not available, this potential flow has been computed by Humphrey, *et al.* (1977). The potential-flow pressure P is needed to start this calculation, and for convenience was approximated as follows. The potential flow pressure P on the inner and outer walls was taken from their figure 5(*b*), and then at each streamwise

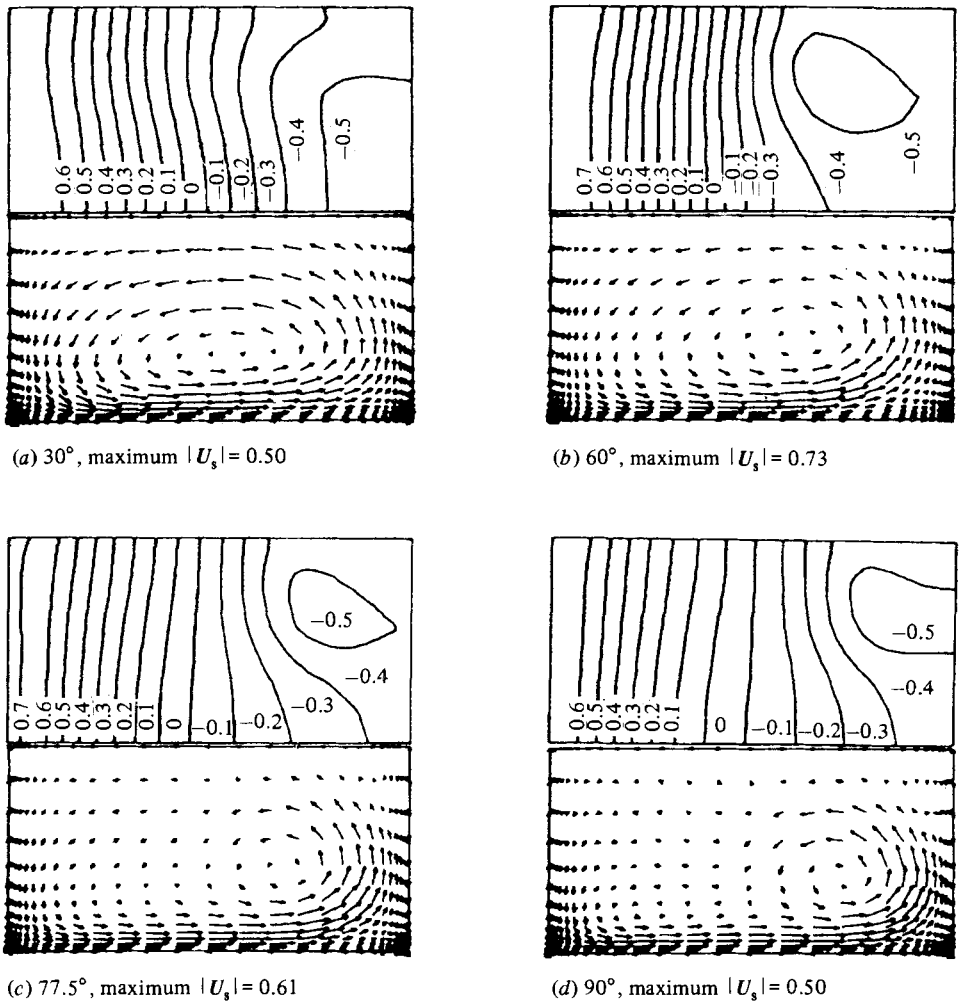

(*a*) 30°, maximum $|U_s| = 0.50$

(*b*) 60°, maximum $|U_s| = 0.73$

(*c*) 77.5°, maximum $|U_s| = 0.61$

(*d*) 90°, maximum $|U_s| = 0.50$

FIGURE 11. Pressure correction Δp (top) and secondary-velocity vectors (bottom) for a 90° bend with $R/d = 2.3$, $Re = 790$, $\delta/d = 0.4$ (inside of bend is to right).

location the potential-flow velocity U was approximated by a profile that varies as r^{-1}, satisfies $Q = 1.0$, and matches the pressure at both inner and outer walls; the pressure P was then obtained from $P = 1 - U^2$. Although the transverse potential velocity W is identically zero for this geometry, the radial potential velocity V is not known and was neglected. This means that the small-scalar-potential approximation is defined relative to the streamwise coordinate instead of the potential flow for this calculation. The initial streamwise vorticity was estimated from the Squire–Winter formula (2.27), using the local transverse vorticity and assuming an average turning angle dx/R of 0.05 rad at the start of the bend, based on the ratio of the measured centreline radial velocity to the mean velocity. This streamwise vorticity distribution was adjusted by the profile shape $f(y_w/\delta)$ prior to initiation of the starting procedure. These approximations in initial conditions and in neglecting V will affect the present comparison somewhat, but should not be very important at downstream locations once large secondary flows have developed and primary flow distortion has occurred.

It was not possible to obtain a complete matching of the inflow velocity distribution, and some adjustment must be made to facilitate the comparison between calculation and measurements. The inflow velocity profiles along both radial ($z = 0.5$) and transverse ($y = 0.5$) coordinates through the duct centreline are shown in figure 8. The present starting profiles did not agree well with measurements unless an adjustment was made in the mass flux used to normalize the computed velocity profiles. When the present reference velocity U_r is reduced by 7 % for the purpose of comparison, the non-dimensional velocity profiles then agree well with measurements (figure 8). The need for this adjustment reflects a 7 % difference between the computed and measured mass flux, which was evaluated here by a second-order accurate integration using the trapezoidal rule. Part of this 7 % difference can be attributed to the form assumed here for the velocity distribution in the corner regions, and part is perhaps due to experimental error. Both adjusted and unadjusted curves are shown here to assist with the comparison.

The behaviour of computed streamwise and radial centreline velocity against streamwise distance is compared with measured data in figure 9. The computed and measured results agree well when adjusted to compensate for the difference in starting conditions (cf. figure 8). The comparison of centreline quantities in figure 9 is believed to be a sensitive indicator of the degree of agreement because it emphasizes the very severe distortion of the streamwise velocity for this case, wherein the streamwise velocity decreases from about 1.7 to about 0.7 within the bend. The peak radial velocity at the centreline is about 0.4.

Computed contours of streamwise velocity (adjusted) are compared in figure 10 with contours derived from the measurements, and the agreement is generally good. Finally, the computed behaviour of secondary velocity and pressure correction $\Delta p (p_m$ is omitted) is shown in figure 11. The computed behaviour of Δp differs significantly from the potential-flow pressure (not shown), which is two-dimensional. The secondary flow is very strong; the peak value of transverse velocity is 0.73 and occurs at the 60° location.

6. Concluding remarks

The goal of the present investigation was to combine physical approximations of acceptable accuracy with the order-of-magnitude improvement in economy of solution derived from non-elliptic approximating equations. When large secondary flows are present, measured static pressures have differed considerably from what is attributable to a potential flow. The present investigation provides some clarification of the extent to which the *difference* in pressure from the (elliptic) potential flow can be represented by a non-elliptic approximation which avoids global iteration in the solution algorithm. It has been shown here that it is not necessary to introduce direct approximations in pressure-gradient terms to obtain non-elliptic equations governing three-dimensional flows with large secondary velocity. The physical approximations made in these non-elliptic equations are suggested by boundary layer order-of-magnitude estimates and are defined as a correction to the potential flow. Although detailed static-pressure measurements were not available owing to the low dynamic head of the laminar flow considered, the present approximations were sufficient to obtain good agreement with measurements of both streamwise and radial velocity components for flow in a square duct with a 90° bend. Although the present results do not provide a definitive assessment of the accuracy or range of applicability of the present approximations, they do suggest that the analysis will prove useful for

many applications, given the considerable economy provided by the non-elliptic approximation.

This work was sponsored by the Computational Fluid Mechanics Branch of NASA Lewis Research Center. The authors are indebted to John P. Kreskovsky and Ralph Levy, who developed portions of the solution algorithm. The thoughtful comments of the referees were also valuable in revising the manuscript.

Appendix A. Classification of approximations in U-, V-, W- and P-variables

It is of interest to compare the results of §3 with similar results for other two- and three-dimensional approximations that have been made in terms of the conventional velocity components and pressure u, v, w and p. The notation is the same as in the main text, except that x-, y-, and z-subscripts denote partial derivatives. The most general approximation considered here is often referred to as the parabolized or thin-layer Navier–Stokes equations, obtained by neglecting only streamwise diffusion terms ($u_{xx} = v_{xx} = w_{xx} = 0$). Only the incompressible Cartesian form of these equations is considered, and all subsequent approximations are classified simultaneously by introducing parameters which allow selected additional terms in these equations to be neglected.

New variables are introduced for transverse velocity gradients as follows:

$$\tilde{U} \equiv u_y, \quad \tilde{V} \equiv v_y, \quad \tilde{W} \equiv w_y, \tag{A 1)–(A 3}$$

$$\hat{U} \equiv u_z, \quad \hat{V} \equiv v_z, \quad \hat{W} \equiv w_z. \tag{A 4)–(A 6}$$

These equations can then be written as the following system of first-order equations:

$$u_x + v_y + w_z = 0, \tag{A 7}$$

$$(\boldsymbol{U}\cdot\boldsymbol{\nabla})\,u + \alpha_1 p_x = Re^{-1}(\tilde{U}_y + \hat{U}_z), \tag{A 8}$$

$$\beta_2(\boldsymbol{U}\cdot\boldsymbol{\nabla})\,v + p_y = \nu_2 Re^{-1}(\tilde{V}_y + \hat{V}_z), \tag{A 9}$$

$$\beta_3(\boldsymbol{U}\cdot\boldsymbol{\nabla})\,w + p_z = \nu_3 Re^{-1}(\tilde{W}_y + \hat{W}_z). \tag{A 10}$$

Subscripted parameters have been introduced in (A 8)–(A 10) for the streamwise pressure-gradient term α_1, and for convective β_2, β_3 and diffusion ν_2, ν_3 terms in the transverse momentum equations. These parameters are assigned values of 0 or 1 according to whether their respective terms are to be neglected or retained in the given approximation.

Although the characteristic equation for the system expressed as (A 1)–(A 10) is degenerate, a nondegenerate first-order system is obtained if (A 1)–(A 6) are replaced by the following six equations, obtained by manipulation of the original system:

$$\tilde{V} \equiv v_y, \quad \hat{W} \equiv w_z, \tag{A 11), (A 12}$$

$$\tilde{V}_z - \hat{V}_y = 0, \quad \tilde{W}_z - \hat{W}_y = 0, \tag{A 13), (A 14}$$

$$\tilde{U}_x + \tilde{V}_y + \tilde{W}_z = 0, \quad \hat{U}_x + \hat{V}_y + \hat{W}_z = 0. \tag{A 15), (A 16}$$

The characteristic equation for this system is given by

$$Re^{-2}\lambda_x^2\lambda_y\lambda_z(\lambda_y^2+\lambda_z^2)^2[\alpha_1\nu_2\nu_3\lambda_x^2 + \nu_3\lambda_y^2 + \nu_2\lambda_z^2] = 0. \tag{A 17}$$

The characteristic equation for the inviscid system given by (A 7)–(A 10) with $Re^{-1} = 0$ is

$$(u\lambda_x + v\lambda_y + w\lambda_z)^2[\alpha_1\beta_2\beta_3\lambda_x^2 + \beta_3\lambda_y^2 + \beta_2\lambda_z^2] = 0. \tag{A 18}$$

The possibility of imaginary roots λ_x is governed by the bracketed term in both (A 17) and (A 18), and two observations comparing these equations with the corresponding characteristic equations (3.12) and (3.13) for the small-scalar-potential approximation are of interest. First, the parameters β_2 and β_3 do not appear in the viscous characteristic equation (A 17), and thus the classification of the viscous approximation does not depend on the treatment of convective terms in the transverse momentum equations; this was also true for the small-scalar-potential approximation. A second observation is that the viscous characteristic equation (A 17) *does* depend on α_1, and hence on the treatment of the streamwise pressure-gradient term. Although the parameter α_1 was not shown in the analysis of §3, the viscous characteristic equation (3.12) for the small-scalar-potential approximation does not depend on the treatment of the streamwise pressure-gradient term. Of course, the inviscid characteristic equations (3.13) and (A 18) depend on the treatment of these convective and pressure-gradient terms, and as discussed previously, this is significant for flow at high Reynolds number.

In the remainder of this Appendix, both convection and diffusion terms in each transverse momentum equation are either retained or neglected together (i.e. $\beta_2 = \nu_2$ and $\beta_3 = \nu_3$). In this case, the bracketed terms in (A 17) and (A 18) are identical, and the classification is the same for both viscous and inviscid forms of the equations. Also, the classification for the two-dimensional form of these equations ($w, \partial/\partial z = 0$) depends on these same bracketed terms, but with the redefinitions $\lambda_z = 0, \beta_3 = \nu_3 = 1$. Several types of flow approximations will now be discussed.

First, in the parabolized or thin-layer Navier–Stokes equations, the only approximation made is to neglect streamwise diffusion terms (all parameters are assigned a value of 1). Since imaginary roots occur in (A 17) and (A 18) for this case, this system of equations is elliptic. If the streamwise pressure-gradient term is suppressed ($\alpha_1 = 0$; all other parameters = 1) then imaginary roots do not occur and the system is non-elliptic. This latter approximation has been widely employed to allow the use of forward-marching algorithms, both as a 'numerical' approximation during global iteration to solve the elliptic system, and as a 'physical' approximation leading to a non-elliptic system. These classifications are the same in two dimensions.

The approximation that neglects both convection and diffusion terms in the y-momentum equation ($\beta_2, \nu_2 = 0$; all other parameters = 1) results in a non-elliptic system. This approximation follows from an assumption that v is small, and gives the boundary-layer equations (plus extra viscous terms in three dimensions) in the form used when the pressure gradients depend on coordinate curvature terms in the y-momentum equation. The slender-channel approximations of Blottner (1977) and Anderson (1980) are of this type.

In three dimensions an assumption that both v and w are small suggests an approximation neglecting convection and diffusion terms in both y- and z-momentum equations ($\beta_2, \beta_3, \nu_2, \nu_3 = 0; \alpha_1 = 1$). However, the characteristic equations (A 17) and (A 18) are degenerate in this case, and this system of equations is insufficient to govern the behaviour of streamwise vorticity. This possibility does not arise in two dimensions. The small-scalar-potential approximation of §2 avoids this difficulty by assuming that v_ϕ and w_ϕ are small, rather than v and w.

Appendix B. Governing equations in orthogonal coordinates

Following algebraic simplification in some instances, the governing equations as approximated in general orthogonal coordinates are given below in the order in which they are solved by the present solution algorithm.

Vorticity equation (2.46)

$$\frac{\rho u}{h_1}\frac{\partial}{\partial x}h_2 h_3 \Omega_1 + \frac{\partial}{\partial y}h_3 \rho v \Omega_1 + \frac{\partial}{\partial z}h_2 \rho w \Omega_1$$
$$+\frac{\partial h_3 \tilde{w}}{\partial x}\frac{\partial}{\partial y}\left(\frac{\rho u}{h_1}\right) - \frac{\partial h_2 \tilde{v}}{\partial x}\frac{\partial}{\partial z}\left(\frac{\rho u}{h_1}\right) - \frac{\partial}{\partial y}(h_3 \rho u^2 K_{13}) + \frac{\partial}{\partial z}(h_2 \rho u^2 K_{12})$$
$$+\frac{\partial \rho v}{\partial y}\frac{\partial \tilde{v}}{\partial z} - \frac{\partial \rho v}{\partial z}\frac{\partial \tilde{v}}{\partial y} + \frac{\partial \rho w}{\partial y}\frac{\partial \tilde{w}}{\partial z} - \frac{\partial \rho w}{\partial z}\frac{\partial \tilde{w}}{\partial y} = Re^{-1}\left[\frac{\partial}{\partial y}\frac{h_3}{h_1 h_2}\frac{\partial}{\partial y} + \frac{\partial}{\partial z}\frac{h_2}{h_1 h_3}\frac{\partial}{\partial z}\right]\mu h_1 \Omega_1. \quad \text{(B 1)}$$

Vorticity definition (2.49)

$$\frac{\partial}{\partial y}\left(\frac{h_3}{h_1 h_2}\frac{1}{\rho}\frac{\partial h_1 \psi}{\partial y}\right) + \frac{\partial}{\partial z}\left(\frac{h_2}{h_1 h_3}\frac{1}{\rho}\frac{\partial h_1 \psi}{\partial z}\right) = -h_2 h_3 \Omega_1 + \frac{\partial}{\partial y}h_3 W - \frac{\partial}{\partial z}h_2 V. \quad \text{(B 2)}$$

Pressure equation (2.47)

$$\left[\frac{\partial}{\partial y}\frac{h_1 h_3}{h_2}\frac{\partial}{\partial y} + \frac{\partial}{\partial z}\frac{h_1 h_2}{h_3}\frac{\partial}{\partial z}\right](P+\Delta p) + \frac{\partial}{\partial y}h_1 h_3 \rho \tilde{C}_2 + \frac{\partial}{\partial z}h_1 h_2 \rho \tilde{C}_3 = 0, \quad \text{(B 3)}$$

where $\tilde{C}_2$ and $\tilde{C}_3$ are given in (2.31) and (2.32). Note that the viscous terms vanish in (B 3), but appear in the boundary condition (4.2).

Energy equation

$$\frac{u}{h_1}\frac{\partial \tilde{E}}{\partial x} + \frac{v}{h_2}\frac{\partial \tilde{E}}{\partial y} + \frac{w}{h_3}\frac{\partial \tilde{E}}{\partial z} = (\rho J Re)^{-1}\left[\frac{\partial}{\partial y}\frac{h_1 h_3}{h_2}\frac{\mu}{Pr}\frac{\partial \tilde{E}}{\partial y} + \frac{\partial}{\partial z}\frac{h_1 h_2}{h_3}\frac{\mu}{Pr}\frac{\partial \tilde{E}}{\partial z}\right]$$
$$+(\rho J Re)^{-1}\left[\frac{\partial}{\partial y}\frac{h_1 h_3}{h_2}\frac{\mu}{2}(1-Pr^{-1})\frac{\partial}{\partial y}(u^2+\tilde{w}^2) + \frac{\partial}{\partial z}\frac{h_1 h_2}{h_3}\frac{\mu}{2}(1-Pr^{-1})\frac{\partial}{\partial z}(u^2+\tilde{v}^2)\right], \quad \text{(B 4)}$$

where $J = h_1 h_2 h_3$. Note that the last term in brackets was omitted in (2.45) and vanishes for $Pr = 1$.

x-momentum (2.35)

$$\frac{u}{h_1}\frac{\partial u}{\partial x} + \frac{v}{h_2}\frac{\partial u}{\partial y} + \frac{w}{h_3}\frac{\partial u}{\partial z} + u(vK_{12}+wK_{13}) - v^2 K_{21} - w^2 K_{31} + (\rho h_1)^{-1}\frac{\partial(P+p_m+\Delta p)}{\partial x}$$
$$= (\rho J Re)^{-1}\left[\frac{\partial}{\partial y}\frac{h_1^2 h_3}{h_2}\mu\frac{\partial}{\partial y}\left(\frac{u}{h_1}\right) + h_1^2 h_3 \mu K_{12}\frac{\partial}{\partial y}\left(\frac{u}{h_1}\right)\right.$$
$$\left.+\frac{\partial}{\partial z}\frac{h_1^2 h_2}{h_3}\mu\frac{\partial}{\partial z}\left(\frac{u}{h_1}\right) + h_1^2 h_2 \mu K_{13}\frac{\partial}{\partial z}\left(\frac{u}{h_1}\right)\right]. \quad \text{(B 5)}$$

State equation (2.44)

$$\rho = (P+p_m+\Delta p)\,\gamma M_r^2 [\tilde{E} - \tfrac{1}{2}(\gamma-1)M_r^2 \tilde{q}^2]^{-1}. \quad \text{(B 6)}$$

Continuity (2.48)

$$\frac{\partial}{\partial x}(h_2 h_3 \rho u) + \frac{\partial}{\partial y}\rho\frac{h_1 h_3}{h_2}\frac{\partial \phi}{\partial y} + \frac{\partial}{\partial z}\rho\frac{h_1 h_2}{h_3}\frac{\partial \phi}{\partial z} = -\left[\frac{\partial}{\partial y}(h_1 h_3 \rho V) + \frac{\partial}{\partial z}(h_1 h_2 \rho W)\right]. \quad \text{(B 7)}$$

REFERENCES

ANDERSON, O. L. 1980 Calculation of internal viscous flows in axisymmetric ducts at moderate to high Reynolds numbers. *Comp. Fluids* **8**, 391–441.

ANDERSON, O. L. & HANKINS, G. B. 1981 Development of a parabolic finite difference method for 3-D high Reynolds number viscous internal flows. In *Computers in Flow Predictions and Fluid Dynamics Experiments*, 119–128. ASME.

BAKER, A. J. & ORZECHOWSKI, J. A. 1983 An interaction algorithm for three-dimensional turbulent subsonic aerodynamic juncture region flow. *AIAA J.* **21**, 524–533.

BLOTTNER, F. G. 1977 Numerical solution of slender channel laminar flows. *Comp. Meth. Appl. Mech. & Engng* **11**, 319–339.

BRILEY, W. R. 1974 Numerical method for predicting three-dimensional steady viscous flow in ducts. *J. Comp. Phys.* **14**, 8–28.

BRILEY, W. R. & MCDONALD, H. 1977 Solution of the multidimensional compressible Navier–Stokes equations by a generalized implicit method. *J. Comp. Phys.* **23**, 372–397.

BRILEY, W. R. & MCDONALD, H. 1980 On the structure and use of linearized block ADI and related schemes. *J. Comp. Phys.* **34**, 54–73.

BRILEY, W. R., MCDONALD, H. & SHAMROTH, S. J. 1983 A low Mach number Euler formulation and application to time-iterative LBI schemes, *AIAA J.* **21**, 1467–1469.

CARETTO, L. S., CURR, R. M. & SPALDING, D. B. 1973 Two numerical methods for three-dimensional boundary layers. *Comp. Meth. Appl. Mech. & Engng* **1**, 39–57.

COURANT, R. & HILBERT, D. 1966 *Methods of Mathematical Physics*, vol. II. Interscience.

DAVIS, R. T. & RUBIN, S. G. 1980 Non-Navier–Stokes viscous flow computations. *Comp. Fluids* **8**, 103–131.

GARABEDIAN, P. R. 1964 *Partial Differential Equations*. Wiley.

GHIA, K. N., GHIA, U., SHIN, C. T. & REDDY, D. R. 1981 Multigrid simulation of asymptotic curved-duct flows using a semi-implicit numerical technique. In *Computers in Flow Predictions and Fluid Dynamics Experiments*, pp. 11–25. ASME.

GHIA, K. N. & SOKHEY, J. S. 1977 Laminar incompressible viscous flow in curved ducts of regular cross-sections. *Trans ASME* I: *J. Fluids Engng* **99**, 640–648.

GOLDSTEIN, R. J. & KREID, D. K. 1967 Measurement of laminar flow development in a square duct using a laser-doppler flowmeter. *Trans. ASME. E*: *J. Appl. Mech.* **34**, 813–818.

HAH, C. 1983 A Navier–Stokes analysis of three-dimensional tubulent flows inside turbine blade rows at design and off-design conditions. *ASME Paper* 83-GT-40.

HAWTHORNE, W. R. 1951 Secondary circulation in fluid flow. *Proc. R. Soc. Lond.* A **206**, 374–387.

HORLOCK, J. H. & LAKSHMINARAYANA, B. 1973 Secondary flows: theory, experiment, and application in turbomachinery aerodynamics. *Ann. Rev. Fluid Mech.* **5**, 247–280.

HUMPHREY, J. A. C., TAYLOR, A. M. K. & WHITELAW, J. H. 1977 Laminar flow in a square duct of strong curvature. *J. Fluid Mech.* **83**, 509–527.

JOHNSTON, J. P. 1960 On the three-dimensional turbulent boundary layer generated by secondary flow. *Trans. ASMED*: *J. Basic Engng* **82**, 233–248.

KHOSLA, P. K. & RUBIN, S. G. 1983 A composite velocity procedure for the compressible Navier–Stokes equations. *AIAA J.* **21**, 1546–1551.

KRESKOVSKY, J. P., BRILEY, W. R. & MCDONALD, H. 1981 Analysis and Computation of Three-Dimensional Flow in Strongly Curved Ducts, In *Computers in Flow Predictions and Fluid Dynamics Experiments*, pp. 129–140. ASME.

LAKSHMINARAYANA, B. & HORLOCK, J. H. 1973 Generalized expressions for secondary vorticity using intrinsic coordinates. *J. Fluid Mech.* **59**, 97–115.

LEVY, R., BRILEY, W. R. & MCDONALD, H. 1983 Viscous primary/secondary flow analysis for use with nonorthogonal coordinate systems. *AIAA Paper* 83–0556.

MOORE, J. & MOORE, J. G. 1979 A calculation procedure for three-dimensional viscous compressible duct flow. Parts I and II. *Trans. ASME* I: *J. Fluids Engng* **101**, 415–428.

PATANKAR, S. V. & SPALDING, D. B. 1972 A calculation procedure for heat, mass, and momentum transfer in three-dimensional parabolic flows. *Intl J. Heat Mass Transfer* **15**, 1787–1805.

PRATAP, V. S. & SPALDING, D. B. 1976 Fluid flow and heat transfer in three-dimensional duct flows. *Intl J. Heat Mass Transfer* **19**, 1183–1187.

PULLIAM, T. H. & STEGER, J. L. 1980 Implicit finite-difference simulations of three-dimensional compressible flow. *AIAA J.* **18**, 159–167.

RALSTON, A. 1965 *A First Course in Numerical Analysis*, McGraw-Hill.

ROBERTS, G. O. 1971 Computational meshes for boundary layer problems. In *Proc. 2nd Intl. Conf. Num. Meth. Fluid Dyn.* (ed. M. Holt). Lecture Notes in Physics, vol. 8, pp. 171–177. Springer.

RUBIN, S. G., KHOSLA, P. K. & SAARI, S. 1977 Laminar flow in rectangular channels. Parts I and II. *Comp. Fluids* **5**, 151–173.

RUBIN, S. G. & REDDY, D. R. 1983 Global PNS solutions for laminar and turbulent flow. *AIAA Paper* 83–1911.

SCHIFF, L. B. & STEGER, J. L. 1980 Numerical simulation of steady supersonic viscous flow. *AIAA J.* **18**, 1421–1430.

STANITZ, J. D., OSBORN, W. M. & MIZISIN, J. 1953 An experimental investigation of secondary flow in an accelerating rectangular elbow with 90 degrees of turning. *NACA TN* 3015.

TAYLOR, A. M. K. P., WHITELAW, J. H. & YIANNESKIS, M. 1982 Curved ducts with strong secondary motion; velocity measurements of developing laminar and Turbulent flows. *Trans ASME* I: *J. Fluids Engng* **104**, 350–358.

VIGNERON, Y. C., RAKICH, J. V. & TANNEHILL, J. C. 1978 Calculation of supersonic viscous flow over delta wings with sharp subsonic leading edges. *AIAA Paper* 78–1137.

WILLIAMS, G. P. 1969 Numerical integration of the three-dimensional Navier–Stokes equations for incompressible flow. *J. Fluid Mech.* **37**, 727–750.